

R & D for the TESLA-Detector: Instrumentation of the very forward region

The Forward Calorimeter Group

Contact Person:
Wolfgang Lohmann

Colorado, Cracow, DESY/Zeuthen, JINR Dubna, London (UC), Minsk (BSU), Prague,
Protvino, Tel Aviv

Summary

In the detector for the TESLA e^+e^- collider the very forward region, i.e. the region directly around the beam pipe in front of the final focus quadrupoles, is a particularly challenging area for instrumentation. A large amount of beamstrahlung, several ten TeV per bunch crossing, is scattered into this region. The distribution of the beamstrahlung has to be measured in order to assist in the tuning of the beams at the final focus. On top of that single, hard electrons have to be measured, or at least vetoed. The latter is important, since events with high energetic electrons near the beampipe are a serious background in many search channels with missing energy and momentum. Outside the area affected by beamstrahlung the region is completed by luminosity monitors, which have to provide the precision measurement of luminosity.

It is the goal of the proposal to carefully investigate the available technological options and to provide a detailed technical design on the timescale of 3 years.

Authors

U. Nauenberg
Physics Department, University of Colorado, Boulder CO USA

D. Kisielewska and L. Suszycki
*Faculty of Physics and Nuclear Techniques, University of Mining and Metallurgy, Cracow
Poland*

A. Eskreys and W. Wierba
Institute of Nuclear Physics, Cracow Poland

E. Kousnetzova, W. Lange, W. Lohmann and A. Stahl
DESY, Zeuthen Germany

A.I. Kalinin, I. Minashvili, D. Mzavia and N.A. Rusakovich
JINR, Dubna Russia

D. Miller
University College, London Great Britain

K. Afanasiev, V. Drugakov, I. Emeliantchik, N. Shumeiko and F. Zyazyula
NC PHEP BSU, Minsk Belarus

O. Kvasnicka and V. Vrba
Inst. of Physics, Acad. of Sciences, Praha Czech Republic

S. Erin, Yu. Gilitzki, V. Korablev, V. Kryshkin, M. Lobanov, V. Suzdalev A. Volkov and
A. Vorobiev
IHEP, Protvino Russia

H. Abramowicz, S. Kananov and Aharon Levy
School of Physics and Astronomy, Tel Aviv University, Tel Aviv Israel

1 Experimental Situation

Goal of the Project

The goal of the project is the instrumentation of the area in front of the quadrupoles, directly around the beam pipe. Figure 1 shows layout of the Detector for the TESLA e^+e^- collider from the Technical Design Report (TDR) [1]. The area under discussion here is indicated on one side of the interaction point by a red circle. There is a similar region on the opposite side. In Figure 2 and 3 this region is shown with more details. Two calorimeters were proposed in the TDR: The LCAL at the innermost radius and the LAT surrounding it. In the studies for the TDR it was assumed that both calorimeters will be constructed as Silicon-Tungsten sandwich calorimeters.

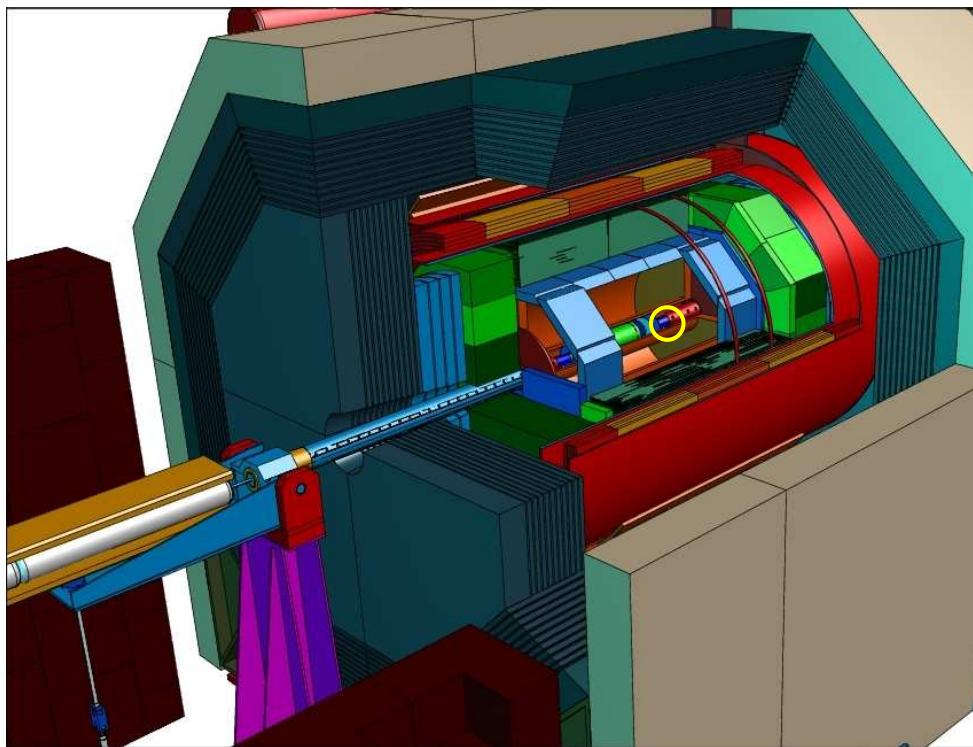


Figure 1: A view on the TESLA detector.

Equipment in the Area

The two calorimeters are mounted inside or in front of a tungsten tube which also acts as shielding of the TESLA-detector against radiation created at the beam pipe. The region will be densely packed with equipment. In the space between the rear end of LCAL and the quadrupole vacuum pumps have to be installed. Also in this region beam position monitors for the fast feedback system need to be mounted. In addition space has to be provided for probably two laser systems: the Shitake monitor for the spotsize of the beams and maybe a Compton polarimeter. And last, but not least space is needed for the readout electronics and support of the two calorimeters.

situation is reversed between electrons and positrons. LCAL is exposed to a large amount of this radiation. The energy deposition is 20 to 40 TeV per bunch crossing and per detector side. For illustration Figure 4 shows the simulation of a few per cent of the background particles resulting from a single bunch crossing. The deposited energy per bunch crossing

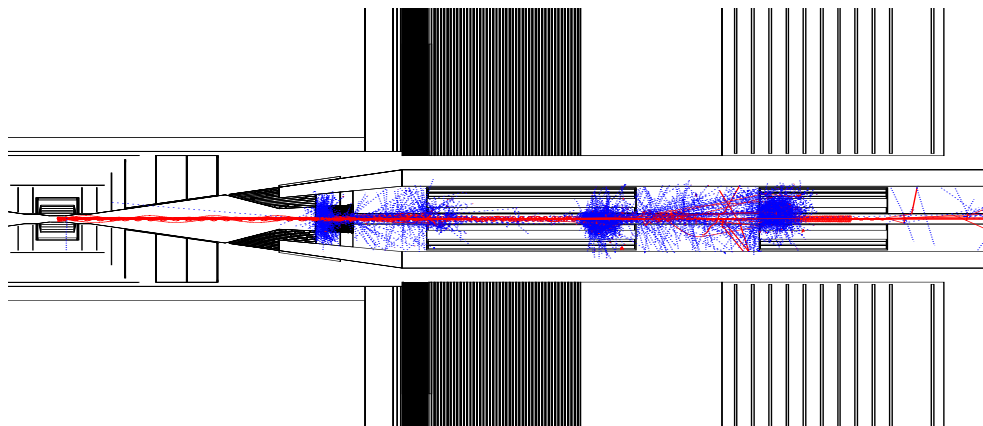


Figure 4: The scheme of the TESLA detector as proposed in the TDR.

in LCAL is shown in Figure 5 as function of the distance from the beam pipe and in the plane perpendicular to the beam direction. It should be mentioned that the amount and

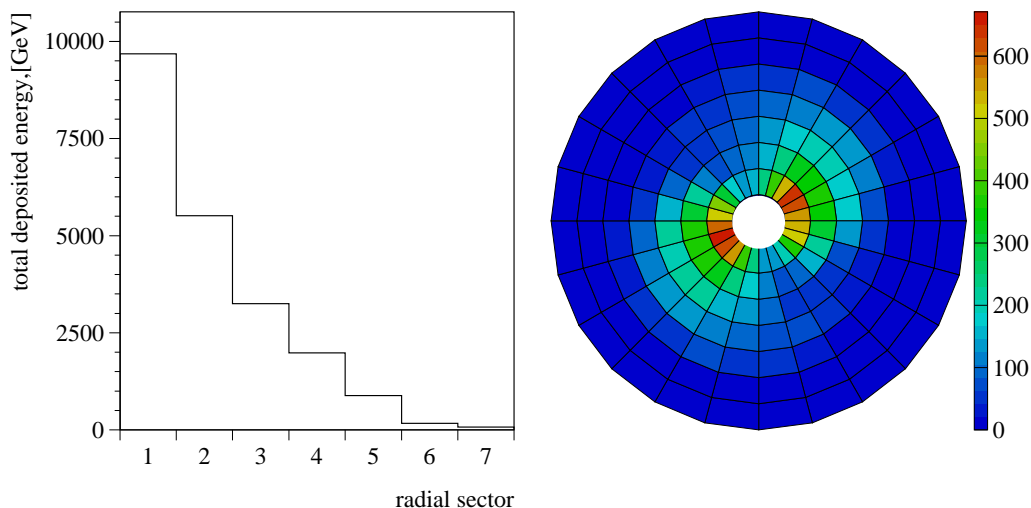


Figure 5: The energy deposition in the LCAL induced by beam background as function of the distance from the beam pipe (left) and in the plane perpendicular to the beam (right). The centre-of-mass energy is 500 GeV and standard machine parameter are used [1]. Each radial sector corresponds to about 1 cm. The units on the right scale are GeV.

distribution of the beamstrahlung remnants strongly depend on the actual beam parameters. They gain transverse momentum up to a maximum value which can be calculated from the size of the electrical field of the oncoming bunch. The deflected particles are contained

within a maximal radius by the magnetic field of the detector. This is roughly 6 cm for the default beam parameters of TESLA in a 3 Tesla solenoidal field. The large amount of beamstrahlung integrates to a substantial amount of radiation dose over the years of operation of TESLA. The total dose expected reaches values of up to 10 MGy/year. This represents a risk of radiation damage to some of the detectors discussed below. LAT is outside the high background region. It is not confronted with these problems.

Required Functionality

The instrumentation in the very forward region has to fulfill a number of tasks:

- Precision luminosity measurement.
- Fast measurement of the distribution of beamstrahlung secondaries. This information is needed in order to optimize the beam parameters at the interaction point during accelerator operation.
- Measurement or at least veto of hard electrons from two-photon events to an as small as possible angle to the beam. If these electrons cannot be detected the events resemble events from new physics with missing energy and momentum. This is the most severe background in some searches.
- Extension of the fiducial volume of the detector for energy flow measurements down to angles close to the beam.
- Shielding of the tracking volume against background resulting from beamstrahlung backscattered from the beam pipe, the quadrupoles, and other equipment positioned downstream.

2 Low Angle Tagger

2.1 General considerations

The Low Angle Tagger(LAT) is expected to give a precision measurement of luminosity, as well as to extend good calorimetric coverage to low angles. To fulfill both tasks, the LAT should have a sufficient depth and longitudinal segmentation and also a fine transversal segmentation.

The luminosity measurement will be based on detection of Bhabha scattering, the process which has proved its functionality for luminosity determination in the LEP experiments [2]. The feasibility of the measurement of the integrated luminosity using LAT has been outlined in [3]. LAT will cover polar angles θ from 27.5 to 83.1 mrad with respect to the beam. The Bhabha scattering cross section amounts to about 5nb and the corresponding event rate will be about 170 Hz ¹. Following the studies for the TDR, it is assumed that LAT will be constructed as a Silicon-Tungsten sandwich calorimeter. The radiation background induced

¹If not stated otherwise, all estimations are based on the nominal TESLA machine parameters, here: beam energy 250 GeV and luminosity $3.4 \cdot 10^{34} \text{cm}^{-2} \text{s}^{-1}$.

by beamstrahlung will be negligible compared to that in the LCAL region and the radiation damage of silicon sensors should not be a problem.

2.2 Monte Carlo simulation

The LAT simulation was performed using a standard GEANT based technique. The whole detector was divided into 14 conical cylinders in r , 24 sectors in the azimuth angle ϕ and 40 cells longitudinally. Each cell was built from a silicon sensor 500 μm thick and a tungsten-silicon mixture composed of 0.34 cm of tungsten and 0.31 cm of silicon. The composition reflects the presence of electronics boards which will be inserted on both sides of each tungsten plate. The resulting cell length is 0.65cm and represents exactly 1 radiation length. Two identical detectors were placed symmetrically with respect to the Interaction Point. The view of the LAT structure is shown in Figure 6.

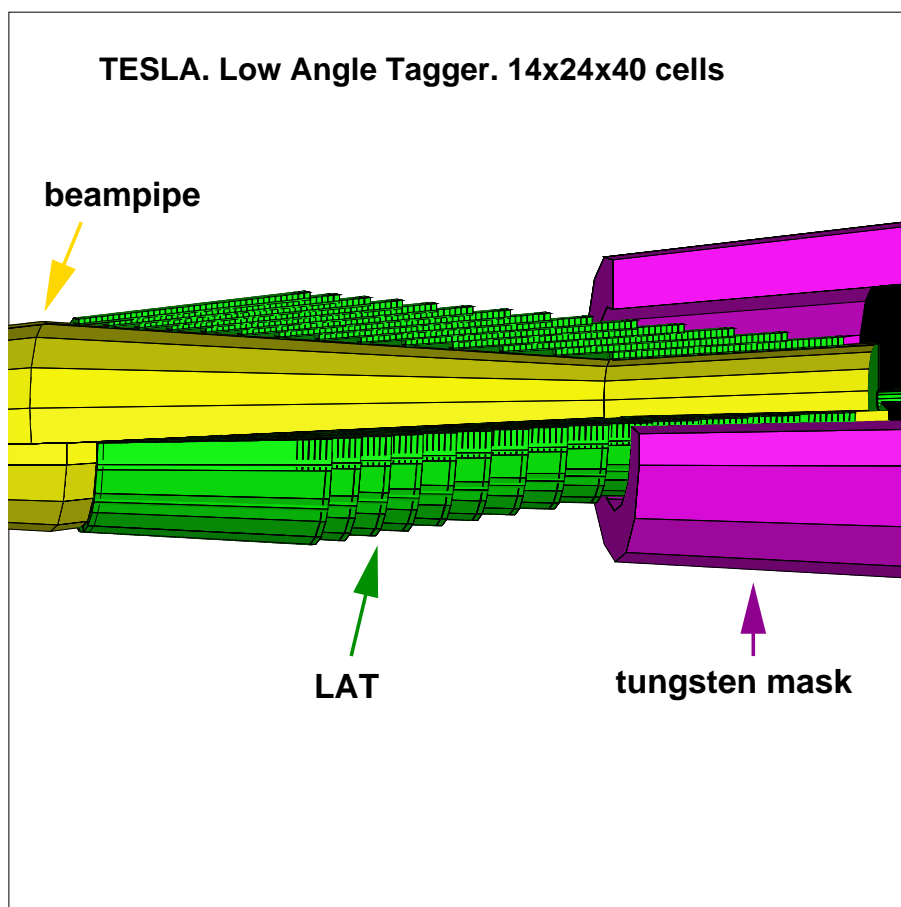


Figure 6: The LAT calorimeter (green). The cut shows its structure. The LAT is mounted just outside the beam pipe (yellow). The tungsten mask (red) and the graphite absorber (black) are also visible.

For a performance study of LAT, electrons were generated in a proper region around the IP with a uniform distribution in θ and ϕ angles. Samples of 400 events were generated at

energies 50, 100, 150, 200, 250 and 400 GeV.

Distributions of the total energy deposited in the silicon sensors are shown in Figure 7. At each energy a tail to low energy deposits is observed, which is due to the particles hitting

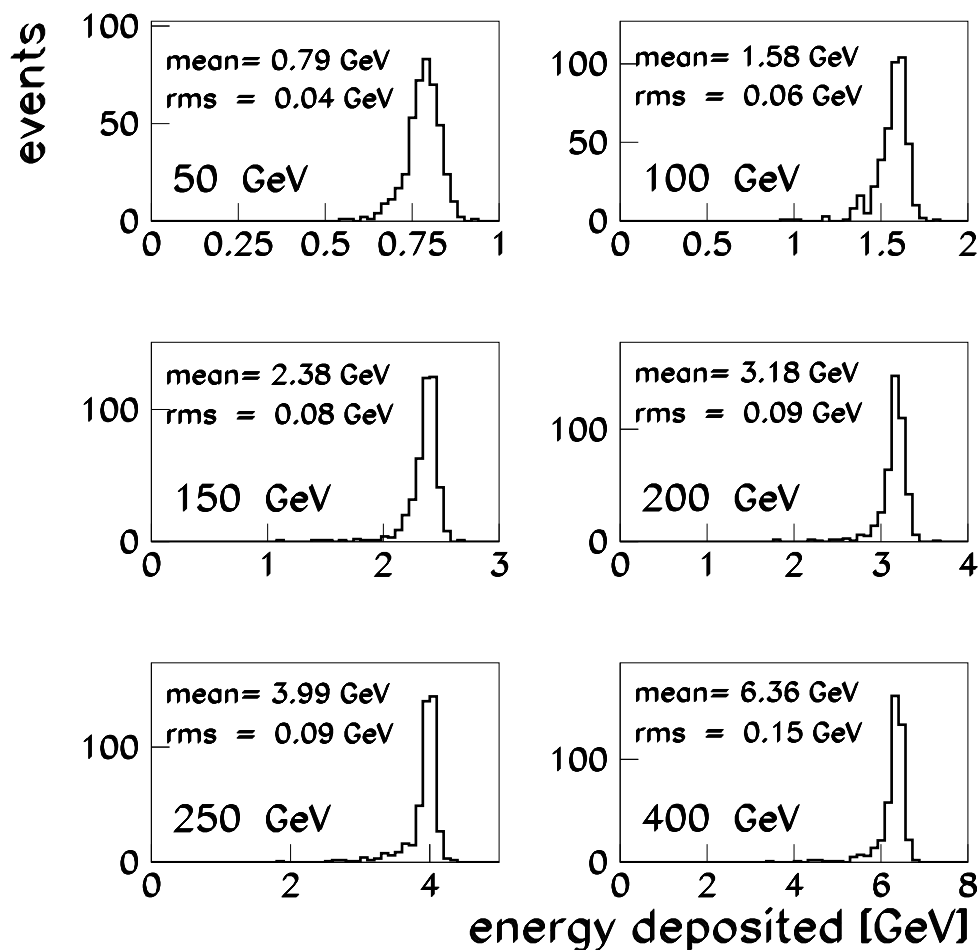


Figure 7: The total energy deposited in the silicon sensors of LAT.

the detector near its edges, at angles close to 27.5 or 83.1 mrad.

The energy response and the energy resolution of LAT are shown in Figure 8. The linearity of response is very good. The energy resolution was fitted to be $\frac{\Delta E}{E} = \frac{37\%}{\sqrt{E}}$. The reason for the rather bad energy resolution was studied in detail. It was found that only 85% of the particle energy is deposited in the bulk of LAT, while the remaining 15% is scattered around. This fraction remains constant with energy. Scanning of events revealed that a large amount of the shower energy is very often smeared over the entire range of the azimuthal angle even up to the side opposite to the incident particle. Future studies will show whether a change of the LAT geometry can reduce the scattered energy.

Figure 9 shows the longitudinal shower profiles and Figure 10 the cumulated energy

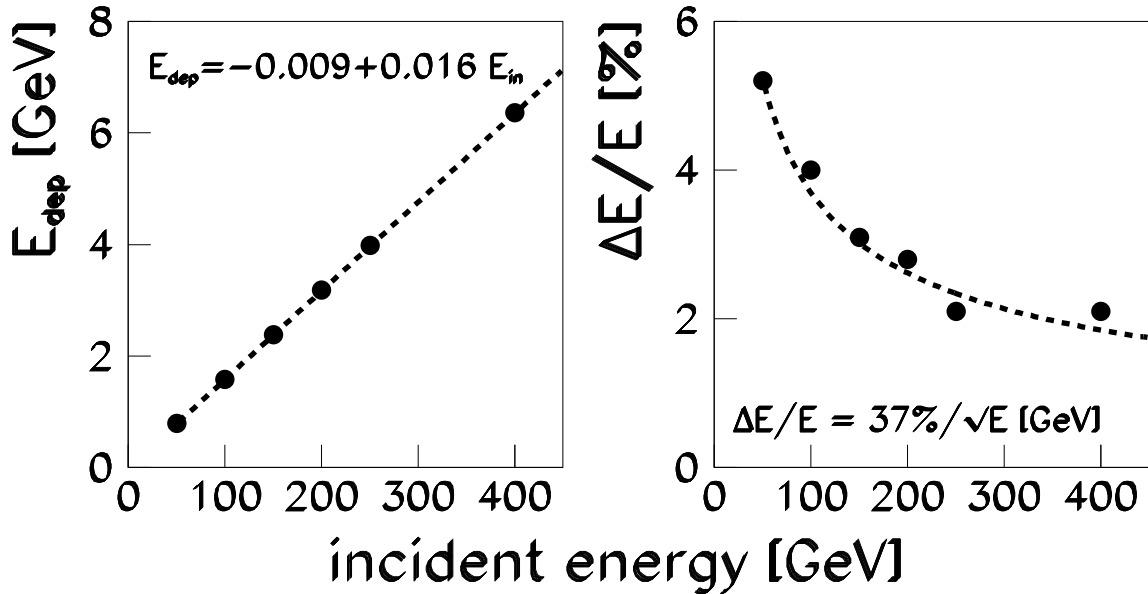


Figure 8: The energy response(left) and the energy resolution(right) of LAT as functions of the particle energy.

fraction deposited up to a given depth. Even at the highest energy of 400 GeV the LAT depth, being at the present study $40 X_0$, is not responsible for energy leakage. The depth can be reduced to $30 X_0$ without significant loss of the energy measurement accuracy.

Dependences of the energy response and the energy resolution on the θ angle were also studied and the results are presented in Figures 11 and 12, respectively. One observes a reduced performance of the detector in the first cylinder corresponding to $\theta = 27.5 - 31.5$ mrad. It could be explained by the edge effects if observed also in the last cylinder at 80 mrad. Since this is not the case, the effect should be studied further for explanation.

The next step is the investigation of the theta angle reconstruction from the distribution of energy deposits in showers. Figure 13 shows the bias $\theta_{gen} - \theta_{rec}$ and the resolution σ_θ as functions of the particle energy. The angular bias is consistent with zero (0.007 ± 0.010 mrad) and the angular resolution is 0.54 ± 0.01 mrad.

Figure 14 presents the same reconstruction parameters as functions of θ . One observes systematic shifts of θ_{rec} to larger values at low angles and to smaller values at high angles. This effect is not understood and has to be investigated.

2.3 Perspectives

The MC results presented here are preliminary. The performance of LAT has to be studied in more detail in order to optimise the detector parameters.

Varying the shape and structure of the detector within limits allowed by the mask the

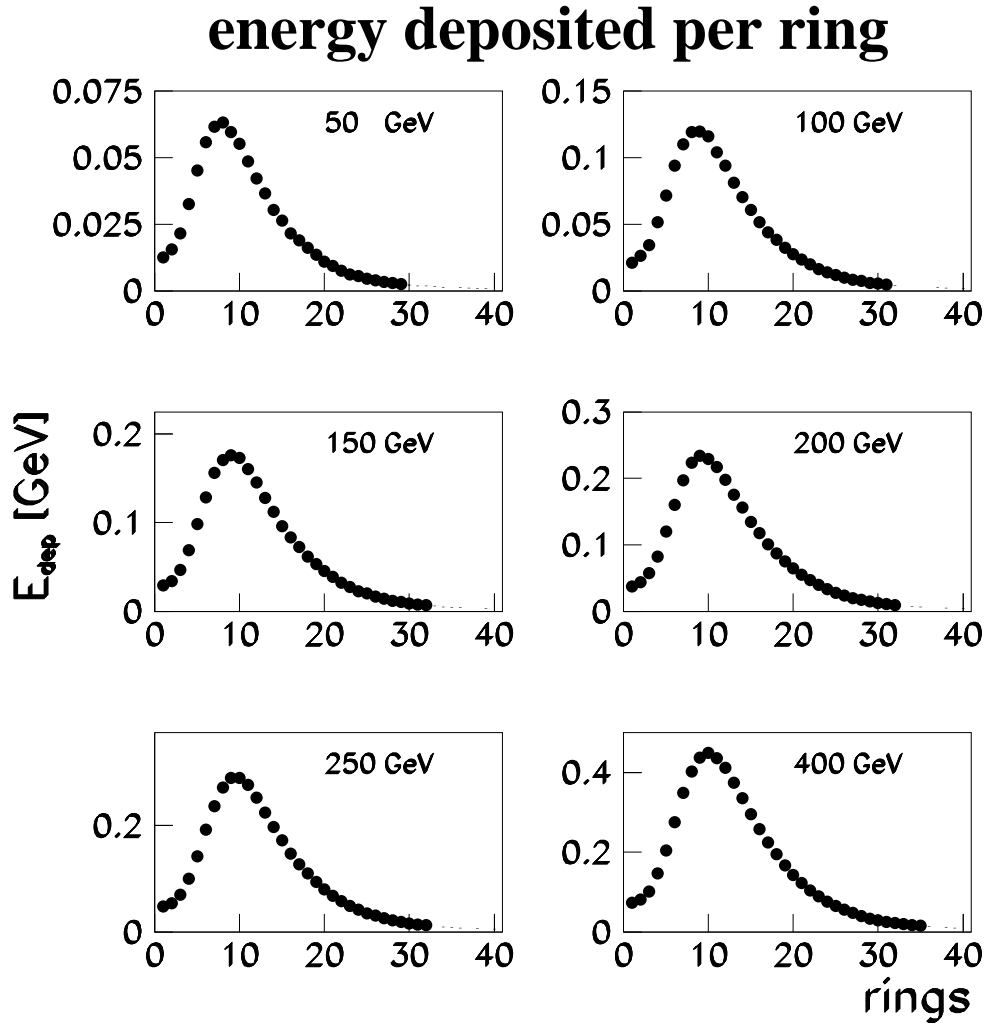


Figure 9: The shower longitudinal profiles in LAT.

solution which offers the best performance will be found. The two alternative structure concepts of LAT, conical and cylindrical, should be simulated and the better one chosen.

Both longitudinal and lateral segmentation of LAT should be refined for improving energy and angular resolutions, but keeping the costs of electronics in reasonable limits.

In order to evaluate the total Bhabha cross section one has to take into account radiative corrections. The present theoretical *state of art* [4] allows to reach a fractional error of about $5 \cdot 10^{-4}$, still larger than the experimental systematic error of $3.4 \cdot 10^{-4}$ as achieved at LEP [2]. Effort from theory groups, e.g. Ref. [5], is ongoing for a better understanding of higher order corrections.

The goal is a LAT design which gives us confidence to approach an experimental precision similar to the theoretical one. Such a design would match the needs *e.g.* of the precision

Energy deposited integral spectrum

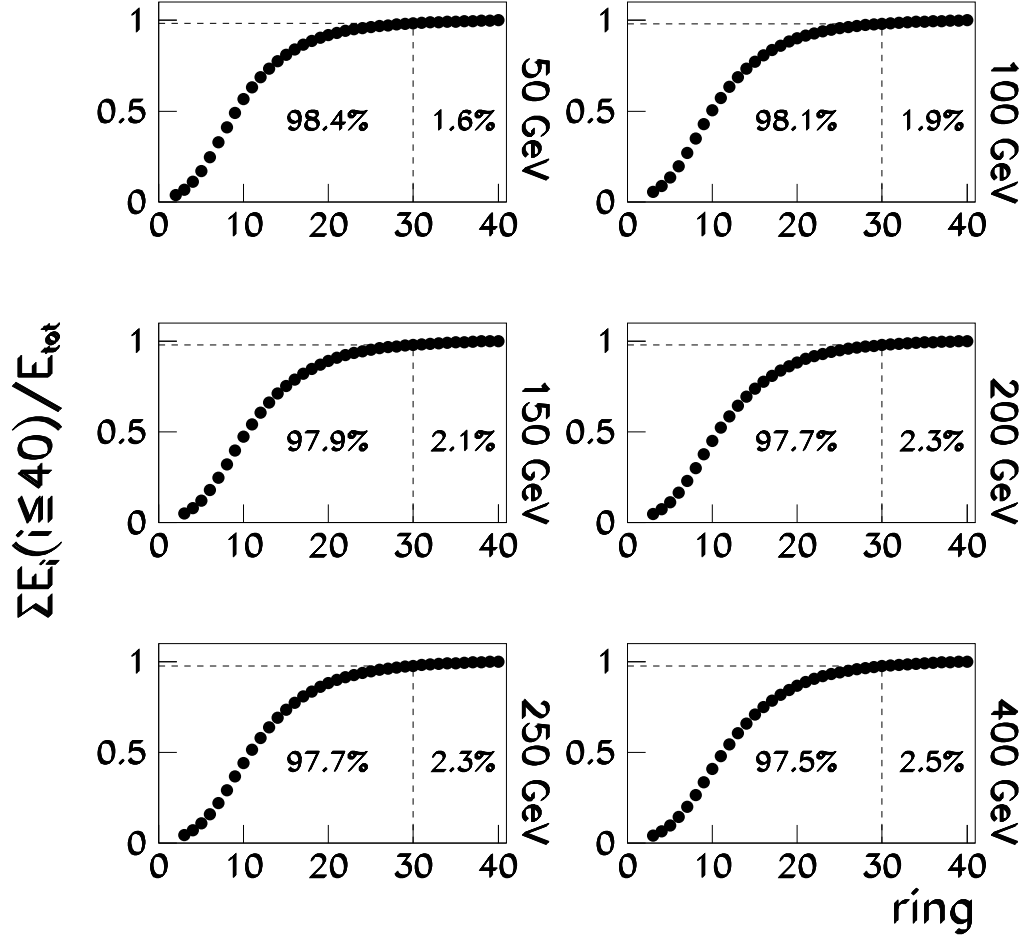


Figure 10: The cumulated energy fraction deposited versus number of layers (“rings”).

measurements of the GigaZ physics program [1].

2.4 Background

Though the level of background originating from beam-beam interactions at LAT will be much lower than at LCAL, several sources of background have to be considered.

Most of the Bhabha scattered electrons² will be accompanied by radiative photons, in other words one will observe bremsstrahlung events $e^+e^- \rightarrow e^+e^-\gamma$.

A check of the theoretical calculations should be possible if the LAT will be able to distinguish hard radiative photons and electrons. To aim this, the first sensor layer is to

²“electron” stands for both electron or positron

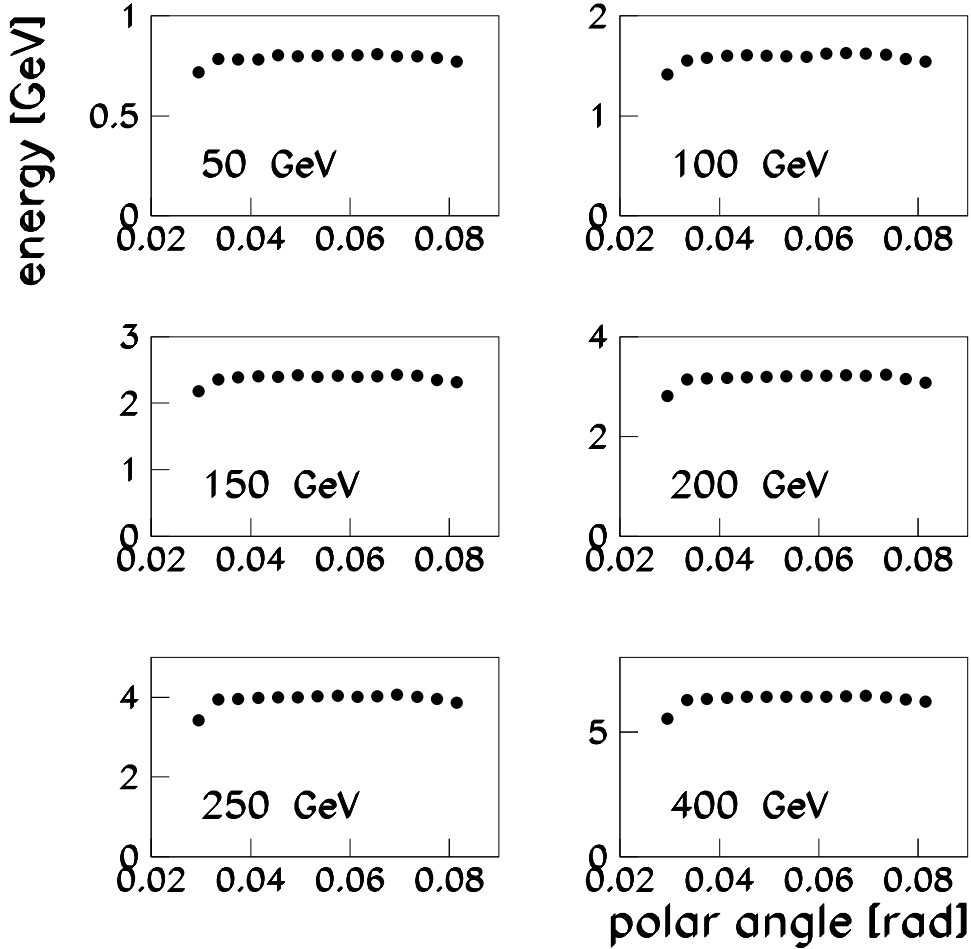


Figure 11: The energy response of LAT as functions of θ for several particle energies.

be placed in front of the first absorber plate in order to distinguish showers induced by a photon from showers induced by an electron.

The very small size of the beam, especially in the vertical direction (5 nm), is the reason to consider also the beam-size effect [6] in the Bhabha cross section calculation.

Another possible source of background at low energies is the back-scattering of thermal photons from the rest gas on the beam, an effect observed at HERA and LEP [7].

Synchrotron radiation produced in the last quadrupole, scattered back on the graphite mask can also give rise to background in LAT.

Last but not least, a background from physics has to be accounted for. Events of the type $e^+e^- \rightarrow \gamma\gamma(\gamma)$, which have the similar experimental signature as Bhabha events are probably the most severe source of background. However, this process can be suppressed if the first layer of the LAT is a sensor layer,

The impact of all these backgrounds on the luminosity measurement will be subject of

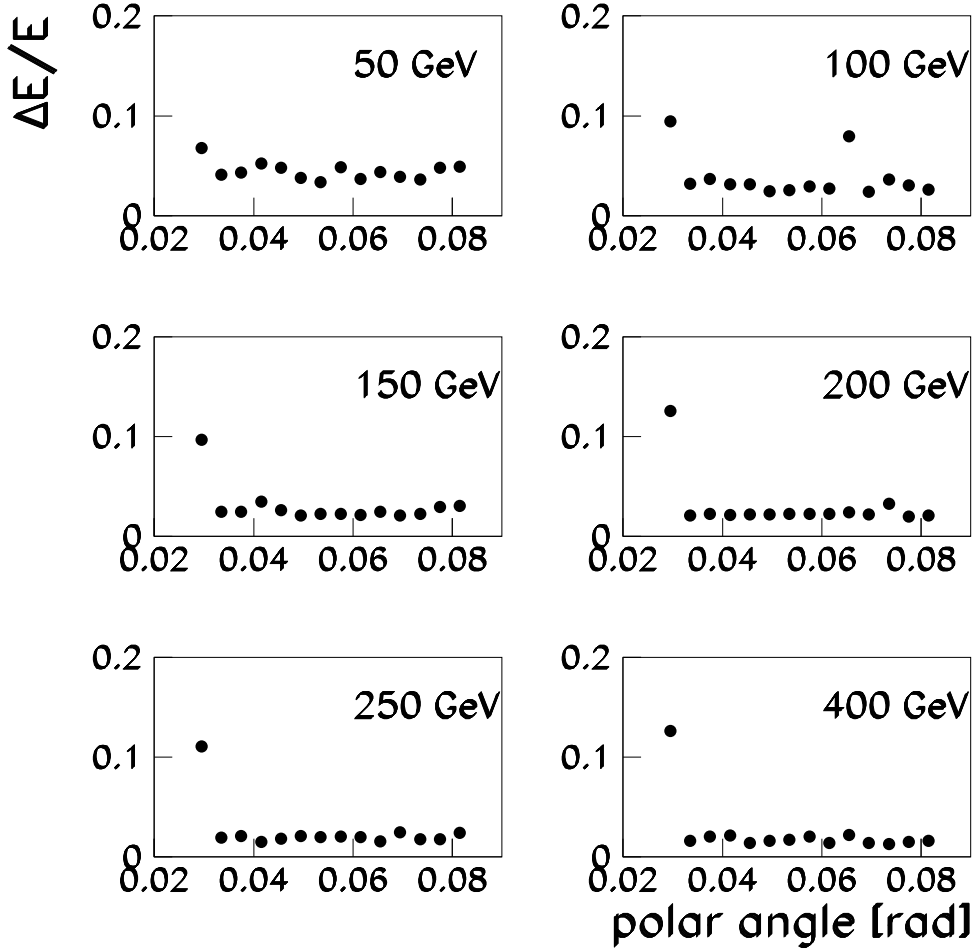


Figure 12: The energy resolution of LAT as functions of θ for several particle energies.

further studies.

2.5 Electronics

The LAT electronics must be carefully designed taking into account the performance benchmarks to be obtained from the more detailed MC studies, the high radiation environment and the limited space in the very forward region. The large number of channels, approximately 20 000, prefers integration of the front-end electronics with the detector. The design will be worked out in close collaboration with the other groups with a benefit of reduced costs.

Angular resolution

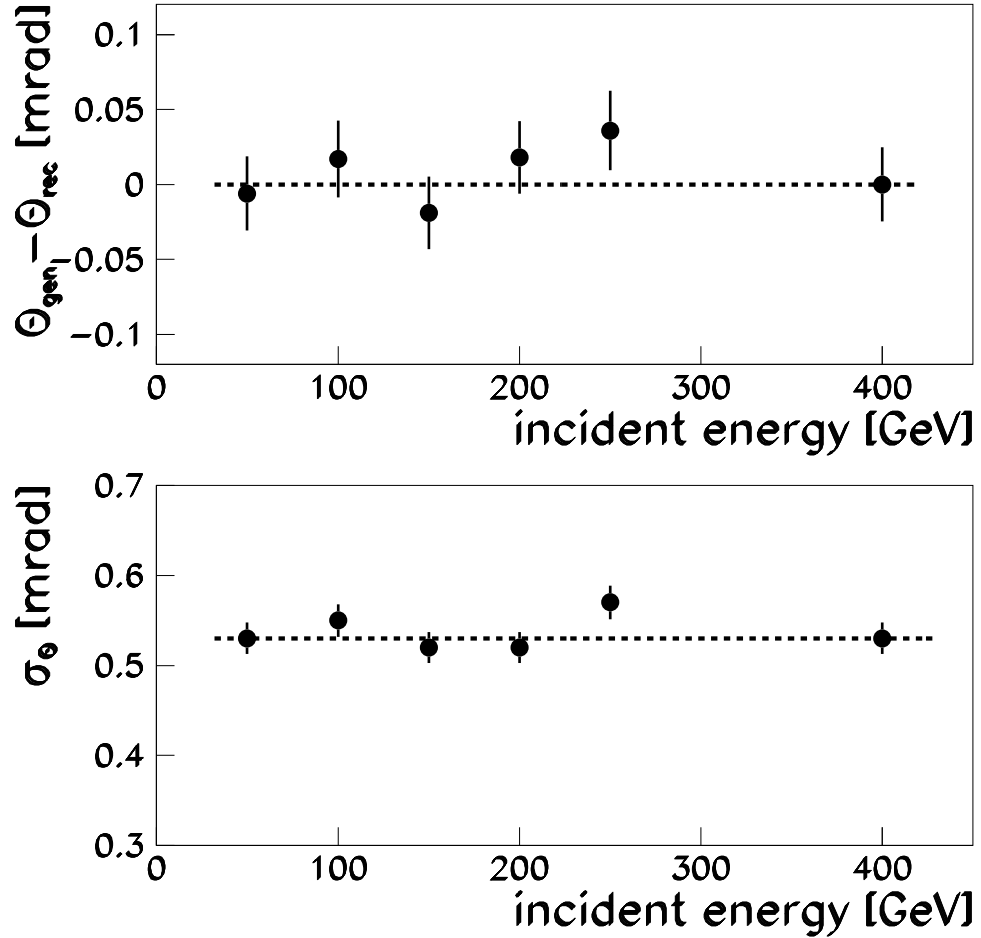


Figure 13: The reconstruction of θ . The difference of the generated and reconstructed angles (left) and the standard deviation of the reconstructed angle (right) as functions of the particle energy.

2.6 Mechanical construction

The LAT construction is a particularly challenging area for the mechanics. Precise measurements of the scattering polar angles forces an ultimate precision in detector metrology.

Based on the results from MC studies a design will be worked out matching the requirements on precision positioning and thermal stability.

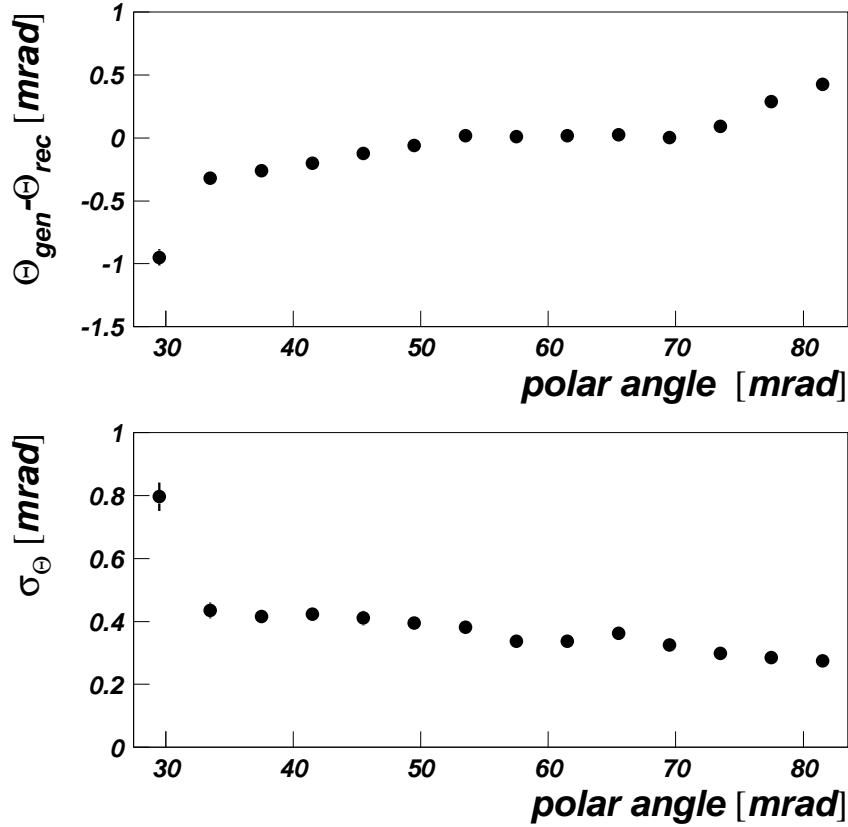


Figure 14: The reconstruction of θ . The difference of the generated and reconstructed angles (left) and the standard deviation of the reconstructed angle (right) as functions the θ angle.

2.7 LAT summary

Further MC studies must be performed to optimise the design of the LAT. The goal is a structure and technology enabling us to measure the Bhabha cross section with a precision of about 10^{-4} . When structure and technology of the LAT are fixed the readout electronics and the mechanical frame will be designed and a prototype segment of the LAT will be prepared for tests.

3 Potential Technologies for LCAL

It is evident that a high granularity is necessary in order to identify individual hard electrons above the background from beamstrahlung. The transversal granularity should not be larger than a Molière radius otherwise an unnecessary high amount of beamstrahlung is integrated into the signal from a hard electron and also position measurement becomes less precise. Also longitudinal segmentation is necessary. The energy deposition of a single 250 GeV

electron differs in the longitudinal shape from the energy deposition of hundreds of .5 GeV electrons from beamstrahlung as can be seen in Figure 15. Hence the analysis of only the

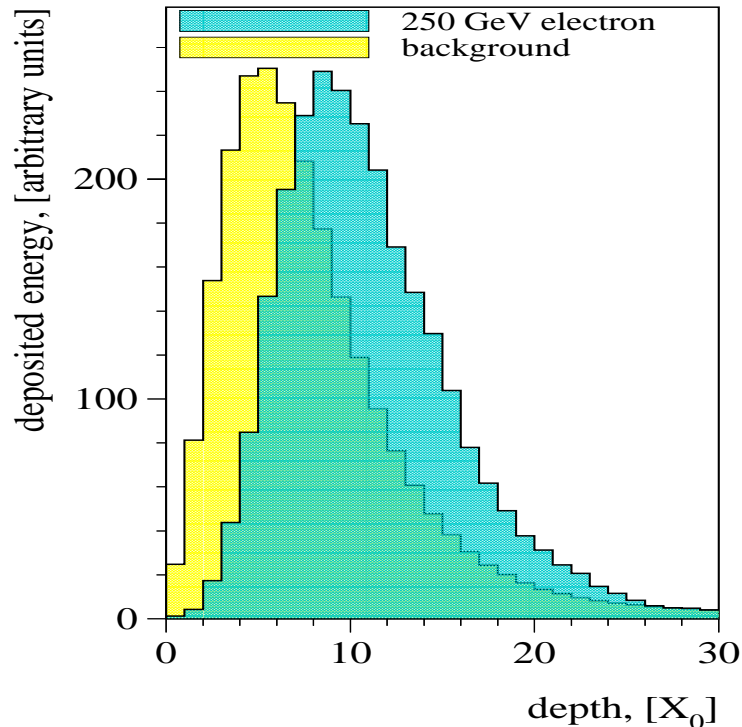


Figure 15: The shapes of the longitudinal energy distributions of electrons from beamstrahlung (background) and a single electron of 250 GeV.

deeper sections of the calorimeter facilitates the identification of a hard electron.

3.1 Silicon-Tungsten or Diamond-Tungsten Sandwich Calorimeter

Silicon-Tungsten calorimeters were successfully used in LEP experiments [2]. The Molière radius is small, typically in the order of a centimeter, leading to very narrow showers for even high energetic electrons.

A possible structure of the calorimeter is sketched in Figure 16. It consists of two half-barrels placed just outside the beampipe. Among the tungsten disks diamond or silicon sensors are interspersed. Because of the large electromagnetic radiation dose silicon sensors might suffer from radiation damage. Diamond sensors are very likely not influenced by large radiation doses [8]. The thickness of the absorber is chosen to be one radiation length and the sensor thickness to be $500 \mu\text{m}$. Variations of the sensor and absorber thicknesses within reasonable ranges change the radiation length and the Molière radius of the detector only weakly, as can be seen from Figure 17. For both materials the sensors are produced as half or quarter discs structured as shown schematically in Figure 18. Silicon sensors could be

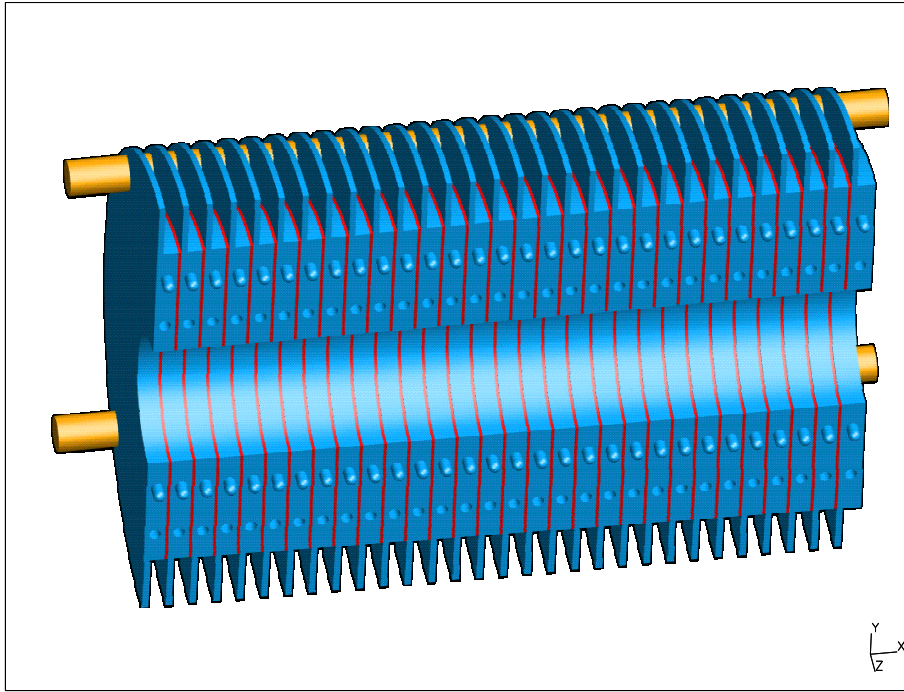


Figure 16: The structure of a half barrel of the sandwich calorimeter. Among the tungsten disks diamond sensors are interspersed.

produced in standard planar technology. Diamond sensors are covered with a metallic layer, where the pad structure is obtained by a lithographic procedure.

The pads of the structured side are read out. Contacts could be made by wire bonding. Each pad is connected by means of a capton flexfoil to charge sensitive preamplifiers. An alternative design would be strips on a second metal layer, which would reduce the total sensor thickness. On the other hand the cross talk from signals in adjacent sensors might be larger compared to the flexfoil readout. In order to cover the large dynamic range of about 1000 each channel could be equipped with two or more amplifiers sharing the input signal charge. The proper preamplifier technology has to be investigated. Options are radiation hard CMOS technology or bipolar amplifiers. As a first prototype existing designs like PRO/A, H1/IDE or as developed for LHC experiments could be used. The preamplifiers will be mounted at the outer rim of the sensors as depicted in Figure 19 and placed in the slots between the tungsten disks as can be seen in Figure 16.

The goal of the R&D project consists of two major parts: the sensor and the readout technology. The steps towards sensor technology will be:

- Test of prototype sensors of the size of several cm^2 from different manufacturers to understand basic features like charge collection distance, homogeneity over the surface and linearity of the response.
- Design, manufacturing and test of prototype sensors covering about a quarter of a ring with a diameter of about 10 cm. In addition to the above mentioned features also the cross talk between pads will be studied for different signal readout techniques.

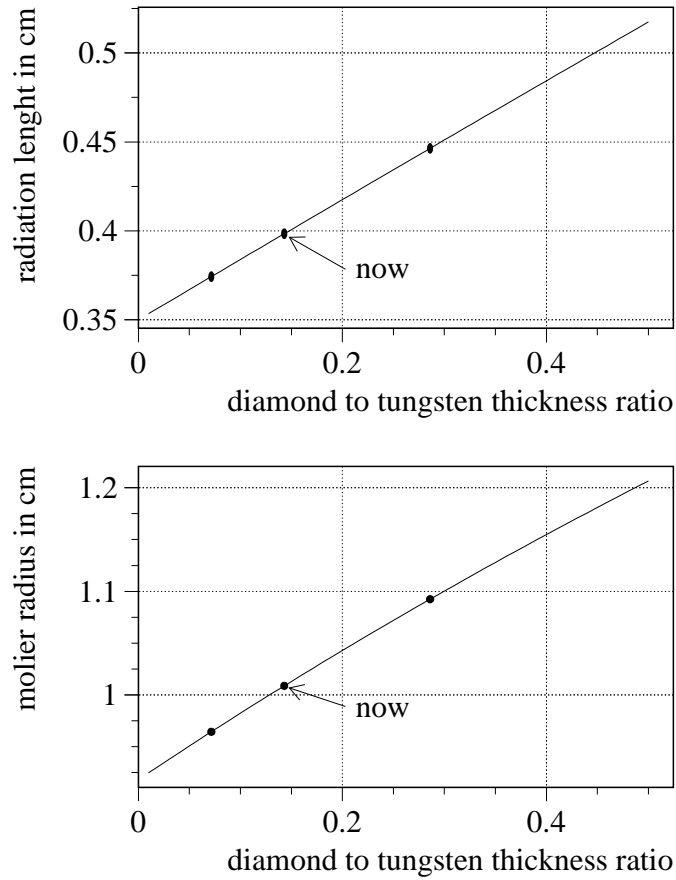


Figure 17: The dependence of the radiation length and the Molière radius on the ratio of sensor and absorber thickness. The arrow points to the current design. The dots left and right indicate the values of the radiation length and Molière radius after changing the thickness ratio by a factor of two.

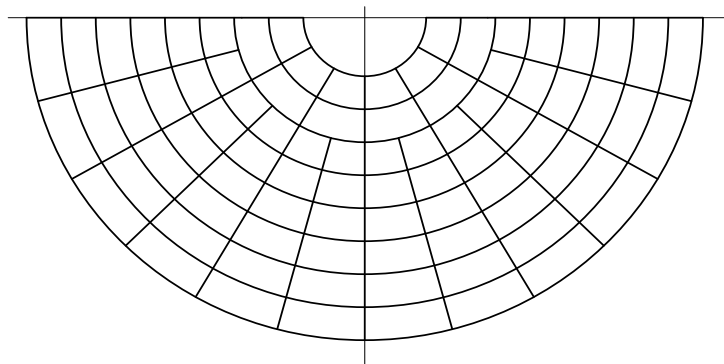


Figure 18: The structure of the sensor surface.

The readout will be done in the first step with preamplifiers of existing designs. In the second

sensor carrier

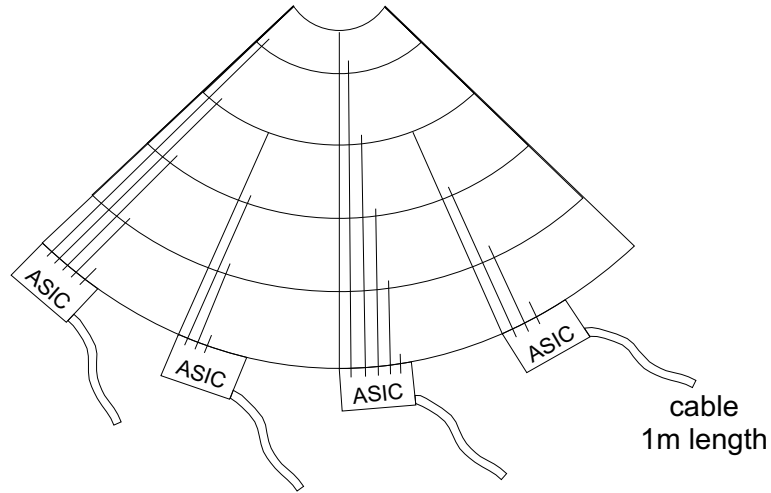


Figure 19: The readout of the sensor pads using a capton printed circuit connected to ASIC preamplifier.

step prototypes will be developed in radiation hard technology adopted to the requirements of the calorimeter and tested with prototype sensors.

If these two parts are finalised successfully a technical design of the calorimeter, including mechanical support and alignment, readout electronics, cooling, calibration and monitoring, will be drawn up.

For the preparation of a prototype segment for testbeam measurements this proposal will be updated.

3.2 Sandwich Calorimeter with Gas Ionisation Chambers

This calorimeter consists of absorber plates similar to the one of the diamond-tungsten calorimeter. The volume between the absorber plates is filled with a heavy gas (e.g. C_3F_8) at overpressure of up to 2 atm, working as an ionisation chamber. The distance between the absorber plates is about 5 mm. In between two absorber plates a PCB layer is placed with a pad structure similar to Figure 18. The absorber plates are grounded and the PCB with pad structure on both sides is on high voltage. The expected features of such a calorimeter are very good linearity over a large signal range, high intrinsic radiation hardness and uniformity of the ionization signal. To monitor the luminosity, the measurement of the current of the gas ionisation will be used. This measurement is available also for beam steering. Some features of such a calorimeter were tested and can be found in reference [9].

The main topics of further studies are:

- Monte Carlo studies to obtain optimal calorimeter performance at small Molière radius

- Gas properties like drift velocity, attachment coefficient, radiation aging for different mixtures.
- Linearity and cross talk between adjacent pads.
- Effect of different pad sizes and grouping of pads into towers for the readout performance.
- Inhomogeneities due to the non-uniformity of electrical field between the boundary of adjacent pads.

A realistic detector prototype will be built to investigate the assembly process, the mechanical properties and the read-out electronics.

3.3 Crystal Calorimeter with Fiber Readout

A homogeneous crystal calorimeter promises better energy and time resolution as compared to a sandwich calorimeter. The Molière Radius has to be kept as low as possible. Therefore the material should be as dense as possible. We are currently thinking about PbWO_4 as scintillator, but even with this scintillator we are still a factor of 2 below tungsten in density and Molière radius.

The standard design of a crystal calorimeter does not provide longitudinal segmentation. The light from a single crystal covering the full depth of the calorimeter is read out from the rear side by a phototube or a photodiode. In order to achieve longitudinal segmentation one might think about cutting the crystal into several pieces in depth and reading each one with a diode. But there is the problem of the nuclear counter effect: Some photodiodes are now operated in the core of the electromagnetic shower. Many charged particles are penetrating the diodes and are creating signals that are much larger than the signals from the light from the scintillator. The calorimeter is effectively transformed into a sampling calorimeter with the crystals as absorbers and the diodes as active sensors. A new idea was brought to our attention by Uriel Nauenberg. The idea is to cut the crystals into pieces and to attach a fiber to every piece of crystal. A possible structure of the calorimeter is shown in Figure 20. Each scintillator piece of a segment is readout by an optical fibre as sketched in Figure 21. The fibers are routed to the back of the calorimeter into an area of low activity and the light from the fibers is read there with multichannel phototubes or avalanche photodiodes. The technology can be used on any crystal calorimeter (at the price of a lower light yield). We want to demonstrate the feasibility of this technology and we want to study its suitability as a technology for LCAL.

The following problems have to be solved:

- Coupling of the light from a small piece of scintillator (typically 1cm x 1cm x 4cm) into a fiber with a reasonable light yield. We are looking at large energy depositions. Therefore the constraints on the light yield are not too tight.
- Identification of a suitable scintillator. PbWO_4 is a good candidate. A crystal with even higher density would still be better. We want to investigate some ideas for new heavy scintillators.

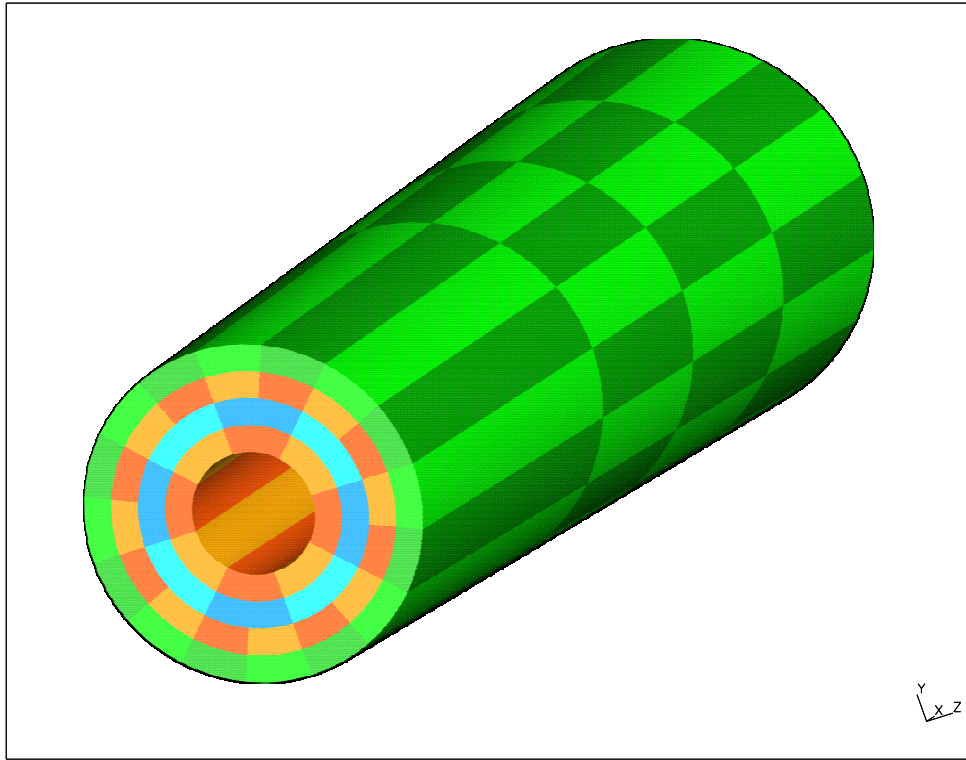


Figure 20: The structure of the crystal calorimeter. The rings consist of segments which are longitudinally subdivided into pieces.

- We need to find fibers with a high radiation hardness. A scintillating fiber would be preferred, because it gives much higher light yields. However, the scintillation process must be fast to avoid negative effects on the time resolution.
- Most crystals create isotropic light through scintillation. In heavy crystals there is light from the Čerenkov effect, even if the crystal doesn't scintillate. We want to investigate whether there are any problems in coupling the directed light from Čerenkov radiation into fibers. It is easier to find a new, denser crystal material, if scintillation is not required.
- For the light readout of the fibers there are two possibilities. Either the fibers are routed along the tungsten pipe to the outside of the TESLA detector. There is no magnetic field there and the fibers could be read by multichannel phototubes. Alternatively one could use avalanche photodiodes and read them directly behind the calorimeter. This solution is more compact, has much shorter fiber lengths (less than 30 cm), but one has to understand the avalanche photodiodes, especially the cross talk.
- A detailed design of the calorimeter has to be made, including mechanical support and alignment, powersupply and readout, cooling, monitoring, etc.

We have started these investigations in Zeuthen. A cosmic telescope has been setup that can measure light yield and time resolution. The test scintillator is interleaved between two

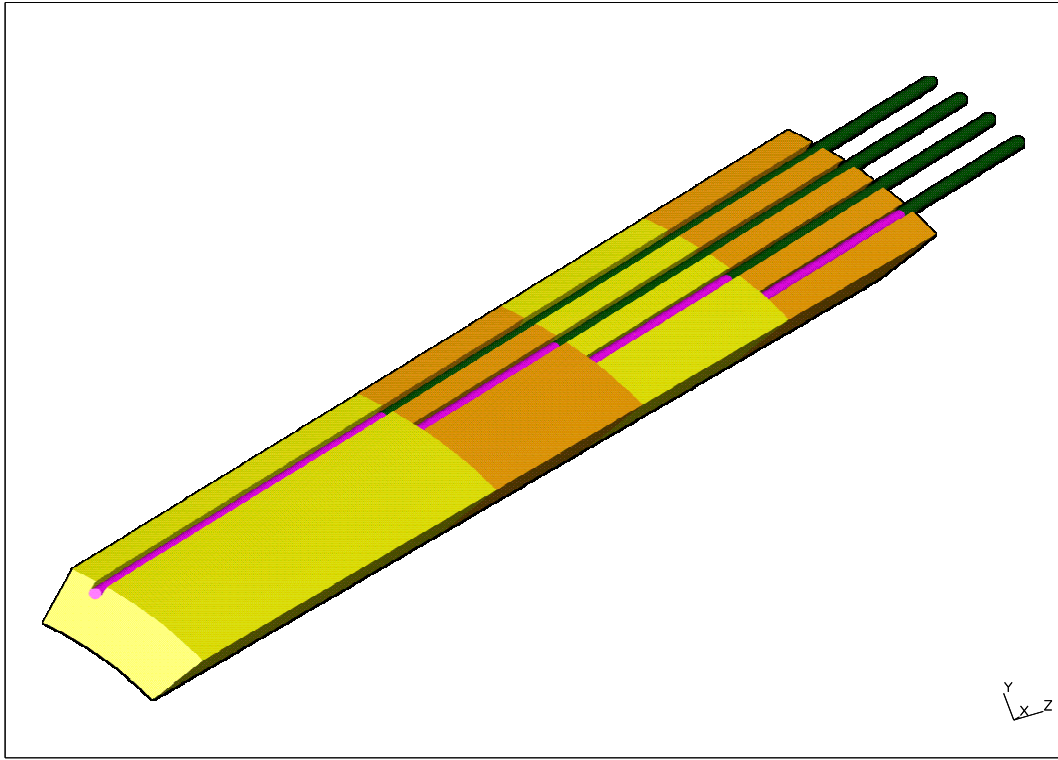


Figure 21: Scintillator pieces forming a segment of the crystal calorimeter. Each piece is connected to an optical fibre, which crosses, optically isolated, the crystals to the rear side of the calorimeter.

trigger counters (Phillips XP 1911 phototubes with plastic scintillators) and a stack of lead to remove low energy muons. The accuracy of the timing measurement was limited by the intrinsic time resolution of the XP1911 tube. Faster tubes (Hamamatsu R7400U) are at hand and are currently being installed.

We have build first test samples with small scintillator pieces and fibers attached to it (typical size 6mm x 6mm x 4 cm). Two students of the Fachhochschule Wildau measured the samples during their practical term. We achieved a lightyield of approximately 30 keV / photoelectron [13]. These first test samples were build from plastic scintillators. A batch of test samples made from lead glass (from OPAL) are ready, but have not been measured yet. We have achieved first experience with avalanche photo diodes. A type of APD provided by MEPhI [14] was investigated. These so-called Silicon Photomultipliers are excellent devices, but their dynamic range was found too small for our purposes.

The plan is to investigate the above question within the next 2 years and – if all can be solved – to build and test a prototype.

3.4 Crystal Calorimeter with Ultrathin Phototriodes

A study of this technology has been performed. Details can be found in ref. [12].

3.5 Preliminary Results from Simulation of LCal

Simulations are done both for a crystal and a diamond tungsten calorimeter. The background stemming from beamstrahlung is generated using the Monte Carlo program Guinea Pig [10]. Single electrons are simulated for different energies and angles. A full shower development is performed using the simulation program BRAHMS [11].

3.5.1 Simulations for the sandwich calorimeter

The structure of the calorimeter is shown in Figure 16. The size of the sensor readout pads is chosen to be about half a Molière radius and the depth of the calorimeter 30 radiation length.

As a first step an average background deposition is defined summing up and averaging the depositions of 10 bunch crossings. For each sensor pad the average energy deposition and the standard deviation is calculated from the signals of the 10 bunch crossings. The result for this average background shape and the standard deviation per pad is shown in Figure 22. Single electrons are simulated with energies between 50 and 250 GeV. The transverse and longitudinal distribution of the energy deposition in the sensors is given as an example in Figure 23 for an electron of 250 GeV. An algorithm is now applied using simulated events consisting of a superposition of the energy depositions of the beam related background and a single electron. From these events an averaged background, as defined above, is subtracted. In the remaining energy depositions a search for local maxima is performed. Only pad signals larger than three times the background standard deviation are accepted. If there are accepted signals in more than 10 longitudinally consecutive pads the deposition is considered as an recognised electron and its energy is reconstructed. The efficiency to detect electrons is shown for several electron energies in Figure 24 for ϕ regions with low and large background. A electron of 250 GeV will be detected even in regions with large background with almost 100%. Electrons of 50 GeV will be identified with high efficiency only at larger radii.

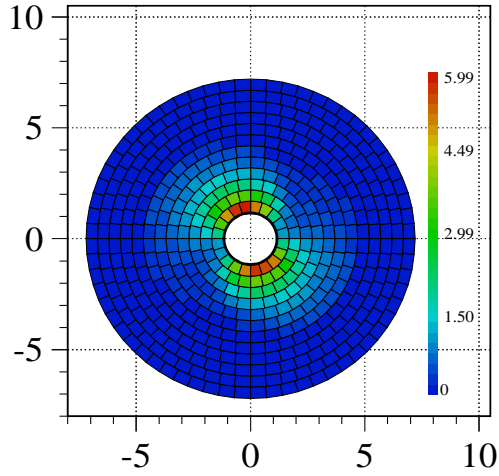
The response of the calorimeter stays almost linear in the range between 50 GeV and 250 GeV, as can be seen from Figure 25.

The energy resolution is expected to be different in regions with low and large background. This is visible in Figure 26. for electron energies of 100 and 250 GeV. Also shown is the resolution obtained in the absence of background and the effect of the digitisation using an ADC with 10 bit resolution. At the innermost ring the degradation of the resolution due to shower leakage is visible. The background deteriorates the resolution in particular at small radii. At larger radii the resolution approaches the expectation for the case of no background. The effect of the digitisation is almost negligible.

Also studied was the rate of fake electrons in e^+e^- annihilations. The first source is of physical nature. The spectrum of electrons from beamstrahlung has a tail to large energies. This can be seen from Figure 27, where the electron energy spectrum above 20 GeV collected over 500 bunch crossings is given. There are a few electrons with energies above 50 GeV which have a chance to be detected in LCal and hence will not be distinguishable from electrons originating from e^+e^- annihilations.

The second source is due to fluctuations in the background. Large local upward fluctuations may lead to an electron-like signature, which is accepted by the algorithm as an electron. For the algorithm described above Figure 27 also shows the spectrum of accepted

TYPICAL LAYER OF AVERAGE BACKGROUND



TYPICAL LAYER OF BACKGROUND RMS

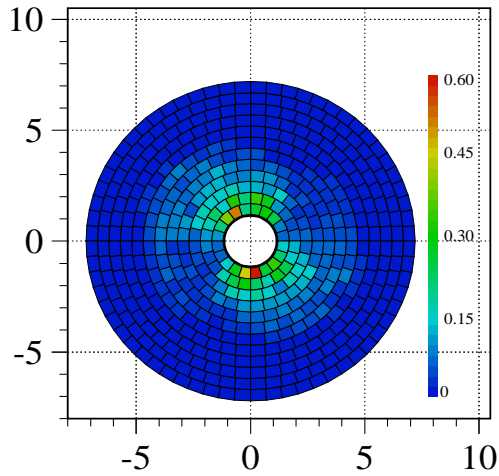


Figure 22: The average background per pad in one layer of the sandwich calorimeter (top) and the standard deviation obtained from 10 bunch crossings (bottom). The scale on the right side is in GeV.

electrons for 500 background events. In addition to the few events expected from high energetic electrons from beamstrahlung some more reconstructed electrons are due to fluctuations, resulting to a rate of about 3% for energies above 50 GeV. For new particle searches this would be an acceptable level.

3.5.2 Simulations for the crystal calorimeter

Similar simulations are done for the crystal calorimeter. Using scintillator pieces made of PbWO_4 the distribution of the energy depositions of a 250 GeV electron for consecutive longitudinal layers is shown in Figure 28. The depositions stemming from beamstrahlung of a single bunch crossing are given in Figure 29. The next two Figures, 30 and 3.5.2, show the superposition of the electron shower and the background, and the depositions remaining after background subtraction. The background distribution for subtraction is obtained from the depositions in the calorimeter on the opposite side of the IP. Again, the energy depositions stemming from the electron can be recognised.

3.6 LCAL Summary

Several promising technologies exist which can potentially be used for fast beam diagnostics and to measure high energetic photons on top of a large electromagnetic background. The goal of the R&D program will be to develop and compare these options. Based on the experience obtained one option will be chosen and a technical design will be worked out including mechanics, cooling, calibration and monitoring.

4 Requests

We ask DESY to support this project as an international collaboration of the institutions listed below. The goal is to develop the key technologies and to find an optimal design for the instrumentation of the forward region. In approximately two years the project will have advanced into a state that we can present a technical design for both forward calorimeters in full detail.

The next step will be the construction of prototype modules of these calorimeters and measurements in the test beam. For these purposes we will update and resubmit this document.

The financial support to perform the project is in the responsibility of the participating laboratories and subject of the applications to their funding agencies. Exceptions are mentioned explicitly. The manpower listed below is expected or foreseen in addition to the authors.

Institution	Contact	Responsibility
Physics Department University of Colorado Colorado / USA	Uriel Nauenberg	Crystal calorimeter
Faculty of Physics and Nuclear Techniques, University of Mining and Metallurgy, Cracow / Poland	Leszek Suszycki Danuta Kisielewska	High precision luminosity measurement – LAT
Institute of Nuclear Physics, Cracow / Poland	Andrzej Eskreys	High precision luminosity measurement – LAT
DESY Zeuthen Germany	Achim Stahl Wolfgang Lohmann	Crystal calorimeter Diamond/tungsten calorimeter
Joint Inst. for Nuclear Research Dubna / Russia	David Mzavia Irakli Minashvili	Crystal calorimeter Diamond sensors
Physics Department University College London / Great Britain	David Miller	LCal technology Luminosity measurement
National Scientific & Educational Center of Particle and High Energy Physics (NC PHEP) Byelorussian State University (BSU) Minsk / Belarus	Nikolai Shumeiko	Simulation of LCAL; Read-out electronics; Diamond and silicon sensors
Institute of Physics Academy of Science Prague / Czech Republic	Vaclav Vrba	Silicon sensors
Institute of High Energy Physics Protvino / Russia	Serguei Erin Viktor Kryshkin	Gas gap calorimeter Diamond/tungsten calorimeter
School of Physics and Astronomy Tel Aviv University Tel Aviv / Israel	Aharon Levy Halina Abramowicz	High precision luminosity measurement – LAT

4.1 Resources LAT

Cracow University of Mining and Metallurgy

- A. Kowal, postdoc (50%), I. Grabowska-Bold, postdoc after June 2003
- One PhD student
- Two technicians

Basic laboratory equipment exists. Additional investments are necessary for calorimeter prototype construction. These investments cannot be covered by Cracow University alone and have to be overtaken by other laboratories. Since these investments will be needed in the second stage of the project a detailed budget plan will be worked out later.

Institute of Nuclear Physics, Cracow

Available manpower is at present 6 physicists and 7 electronics engineers. The engineers are presently occupied almost full time with upgrade of the ZEUS luminosity measurement system but it is intended that gradually over the next 1.5 years at least half of them will be shifted to LAT activities. Standard laboratory equipment is available.

Tel Aviv University

- One MSc student

Standard laboratory equipment is available.

Acad. of Sciences Prague

- Technicians and workshop

An equipped laboratory for sensor testing is available. The group has experience in silicon sensor development and production in collaboration with local partners.

4.2 Resources LCAL: Diamond / Tungsten technology

DESY
Zeuthen

- Support for two diploma students or equivalent
- Support for guests for a total of one year
- Machine shop: 6 weeks for sensor positioning and absorber prototypes, mechanical supports
- Designer (mechanics): 3 months for prototype design
- Electronics engineer: 3 months for prototype design and assembly
- Electronics workshop: 3 months for prototype assembly

Standard laboratory equipment is partly available. The necessary completion will be subject of a separate request to DESY.

JINR
Dubna

- Two physicists
- One engineer
- One technician

Standard laboratory equipment and workshops are available.

NCPHEP BSU
Minsk

- Two electronics engineers

Standard laboratory equipment is available; Prices for test sensors from domestic suppliers are investigated. Expenses will be covered by NCPHEP BSU. In a later stage support from outside is necessary.

IHEP
Protvino

- Two electronics engineers

Standard laboratory equipment is available; also electronics and mechanics workshops. In addition the laboratory operates a facility to produce diamond films. In a later stage support from outside is necessary.

4.3 Resources LCAL: Crystal technology

DESY

- 1 postdoc position for 2 years
50 % involvement in this project 50 % in the TESLA $\gamma\gamma$ collider option.
- Support for 1 or 2 diploma students or equivalent.
- Support for guests for a total of one year.
- Machine shop: 10 weeks of labour for cutting, polishing, glueing of crystal samples.

Standard laboratory equipment is partly available. The necessary completion will be subject of a separate request to DESY

BSU NCPHEP
Minsk

- Two electronics engineers

Standard laboratory equipment is available; Prices for test sensors from domestic suppliers are investigated. Expenses will be covered by NCPHEP BSU. In a later state support from outside is necessary.

JINR Dubna

- Two physicists
- One engineer
- One technician

Standard laboratory equipment is available; access to electronics and mechanics workshops.

4.4 Resources LCAL: Sandwich calorimeter with gas ionisation chambers

IHEP Protvino

- Three students

Standard laboratory equipment is available and access to machine shops exists. Some support for gas purifiers and special electronics is expected from other laboratories.

References

- [1] TESLA Technical Design Report, DESY 2001-011, ECFA 2001-209, March 2001.
- [2] **D. Bédérède et al.** (ALEPH Collaboration), Nucl. Instr. and Meth. **A 265** 117 (1995); **G. Abblendi et al.** (OPAL Collaboration), Eur. Phys. J. **C 14**, 373-425 (2000).
- [3] **K. Buesser, M. Paganoni**, LS notes, LC-DET-2001-044.
- [4] **S. Jadach, W. Placzek, E. Richter-Was, B.F.L. Ward, Z. Was**, Comput. Phys. Commun. **102** (1997) 229.
- [5] **J. Fleischer, T. Riemann, O. Tarasov and A. Werthenbach**, talk at the 'Int. Workshop on linear Colliders', Jeju Island, Korea 2002, <http://www-zeuthen.desy.de/theory/radcor02/>;
S. Jadach, talk at the CLIC workshop, CERN 18/19 December 2001, <http://jadach.home.cern.ch/jadach/>.
- [6] **A. E. Blinov et al.**, Phys. Letters **113B**, 423 (1982); **G.I. Kotkin, V.G. Serbo, A. Schiller**, Int. J. Mod. Phys. A, 4707 (1992).
- [7] **B. Dehning, et al.**, Phys. Letters B **249**, 145 (1990); C. Bini et al., CERN-PPE/91-64, submitted to Physics Letters B.
- [8] **T. Behnke et al.**
Linear Collider Note, LC-DET-2002-001, DESY 2002.
- [9] **S. Denisov et al.**
Submitted to the 8th International Conference On Instrumentation For Colliding Beam Physics (INSTR02) 28 Feb - 6 Mar 2002, Novosibirsk, Russia.

- [10] **D. Schulte**, Thesis, Hamburg 1996.
<http://www-sldnt.slac.stanford.edu/nlc/beamdeliveryhome.htm>.
- [11] **T. Behnke et al.**,
<http://www-zeuthen.desy.de/linear-collider/>.
- [12] **H. Araujo et al.**, LC-DET-2001-080, DESY 2001.
- [13] **N. Conrad, B. Neick**, Praxissemesterbericht, Fachhochschule Wildau. <http://www-zeuthen.desy.de/astahl/vorwaerts.html>.
- [14] **P. Buzhan et al.**, *An Advanced Study of Silicon Photomultiplier*, ICFA Instrumentation Board.

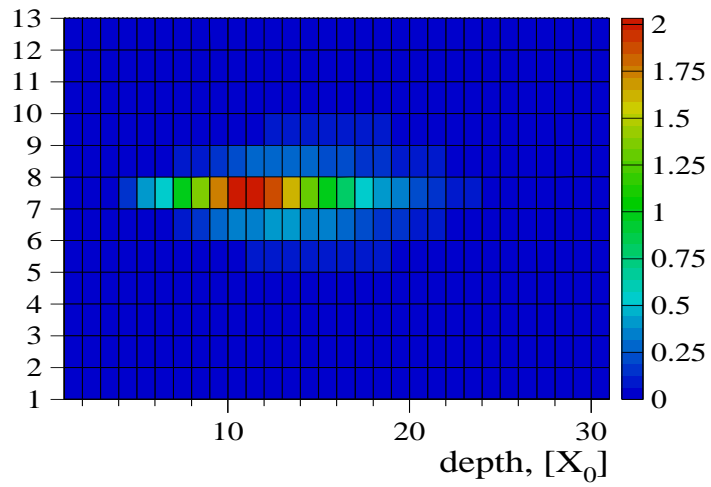
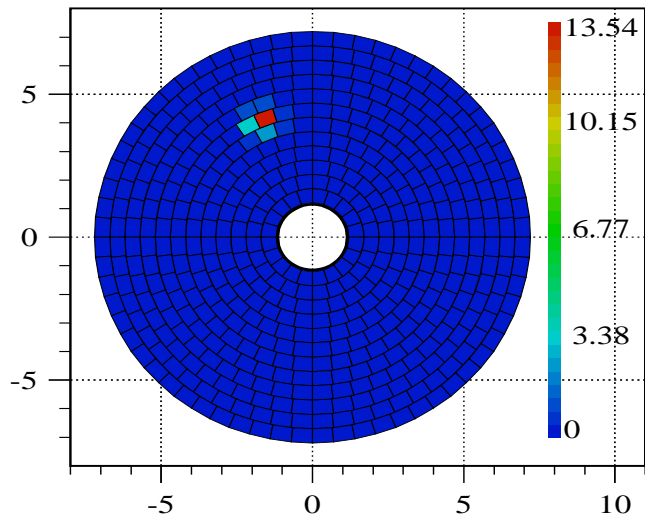


Figure 23: The transversal (top) and longitudinal (bottom) projections of the shower of a 250 GeV electron in the sandwich calorimeter. The scale on the right side is in GeV.

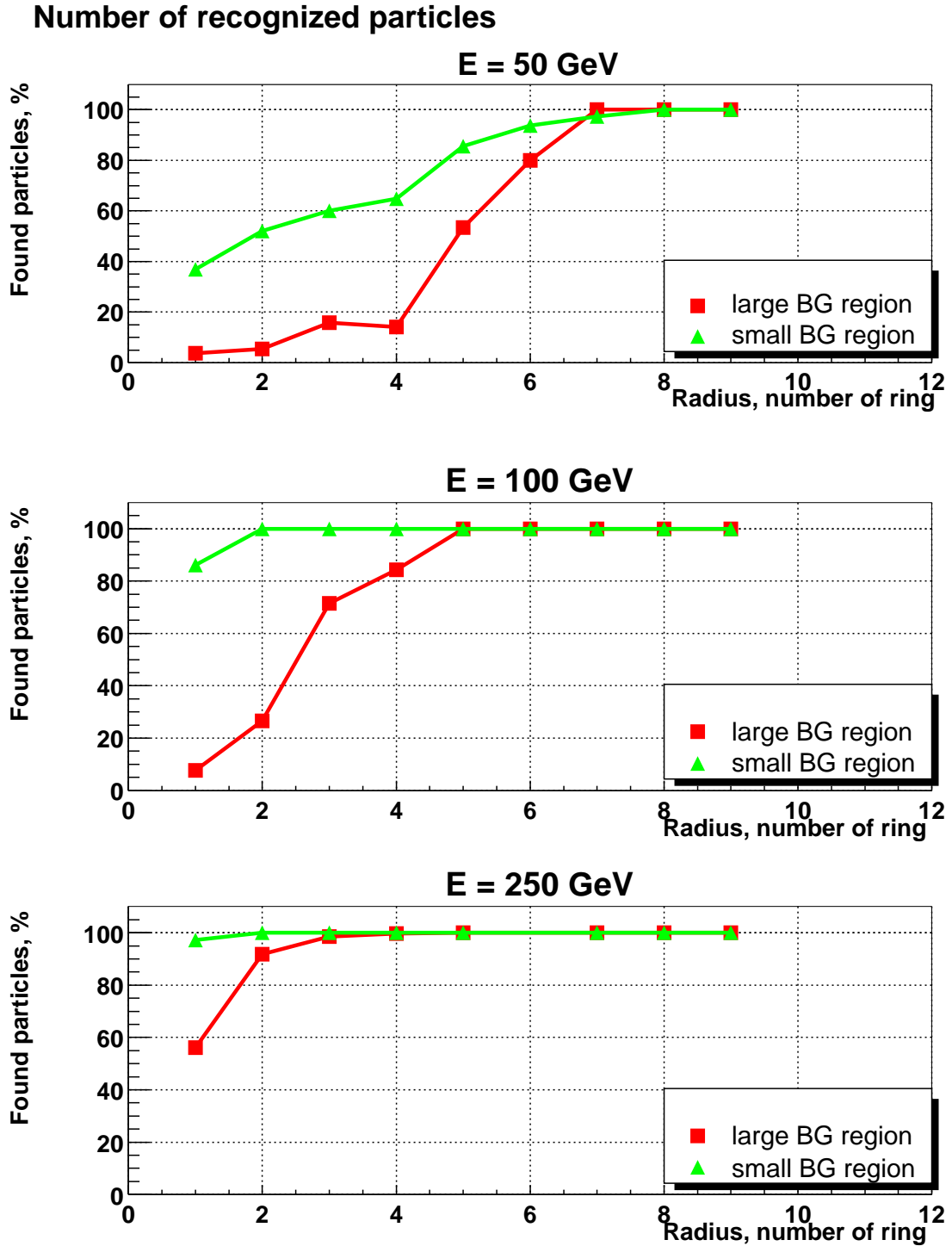


Figure 24: The efficiency to identify an electron of energy 50, 100 and 250 GeV as function of the radius in the large background region (squares) and the low background region (triangles).

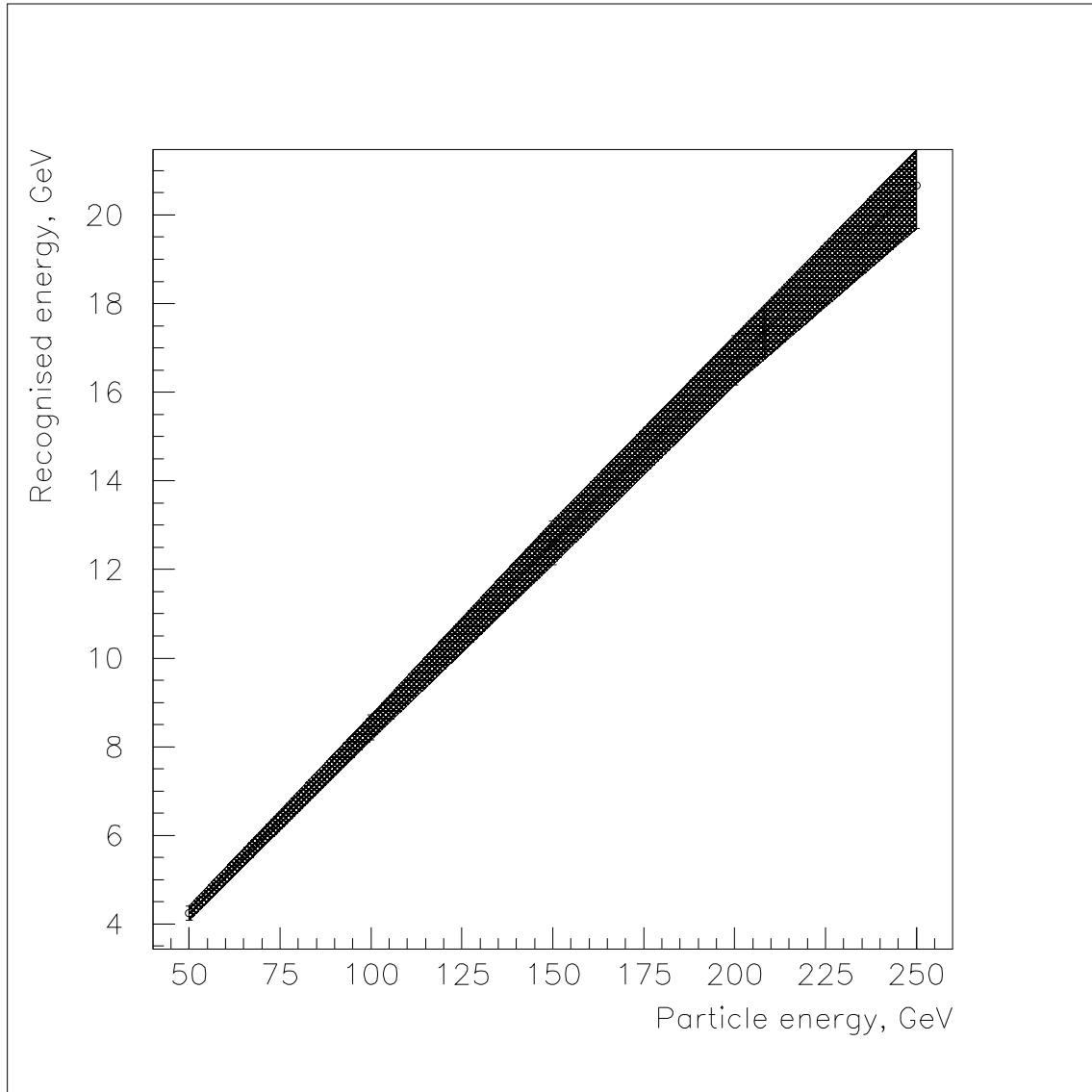
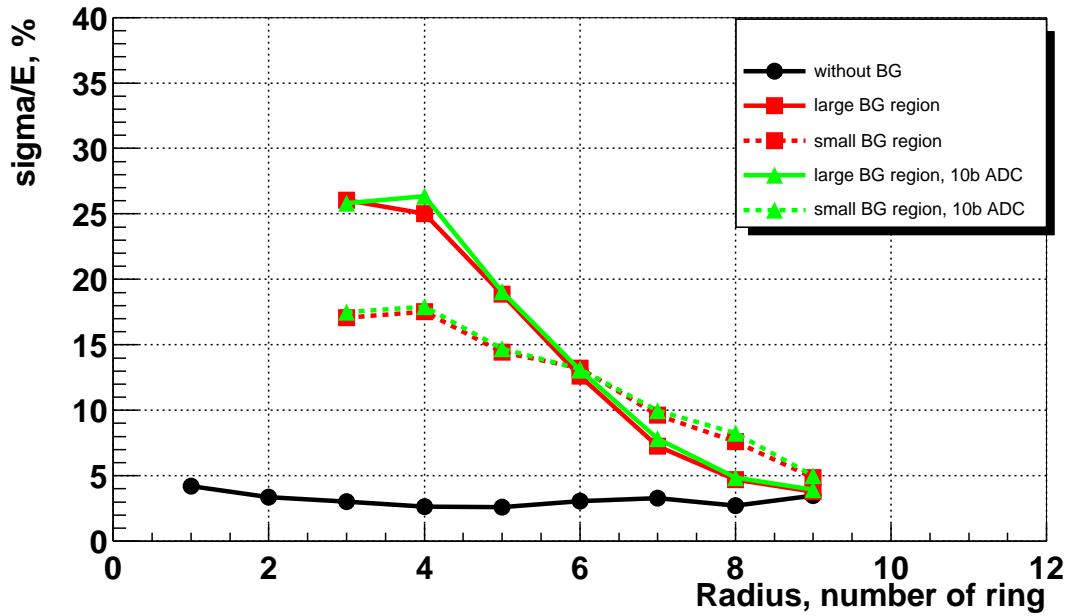


Figure 25: The energy measured in the calorimeter as function of the initial electron energy.

Resolution

E = 100 GeV



E = 250 GeV

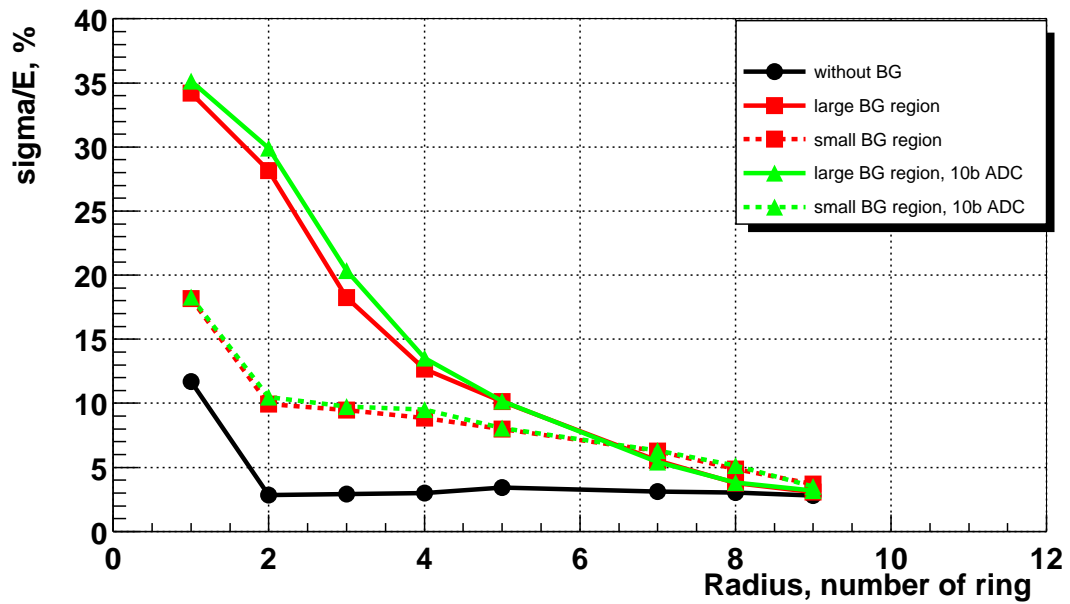


Figure 26: The resolution of the energy measurement in the calorimeter for electron energies of 100 and 250 GeV as function of the radius. Black dots correspond to the case of no background, the dashed lines to the small background and the solid lines to the large background regions. Squares are obtained before and triangles after digitisation using an ADC with 10 bit resolution.

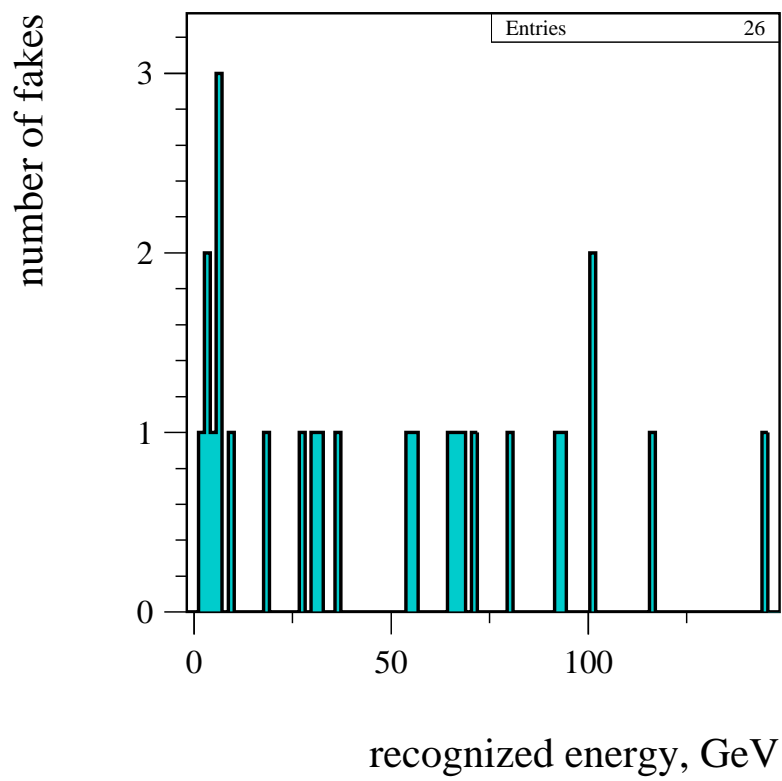
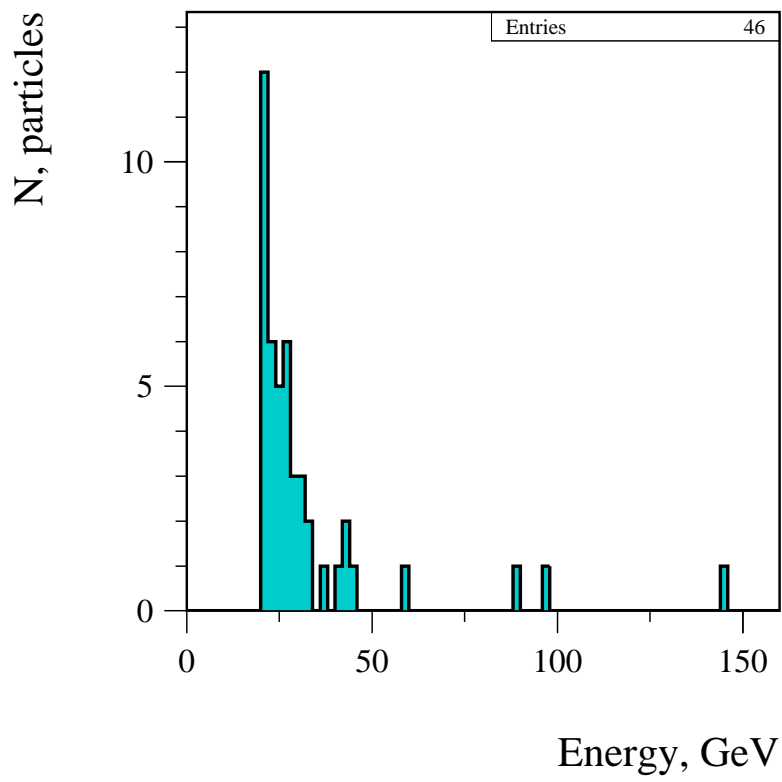


Figure 27: The spectrum of electrons originating from beamstrahlung collected over 500 bunch crossings (top). Electrons with energies below 20 GeV are not considered. The spectrum of reconstructed single electrons in a sample of 500 events of beamstrahlung only (bottom).

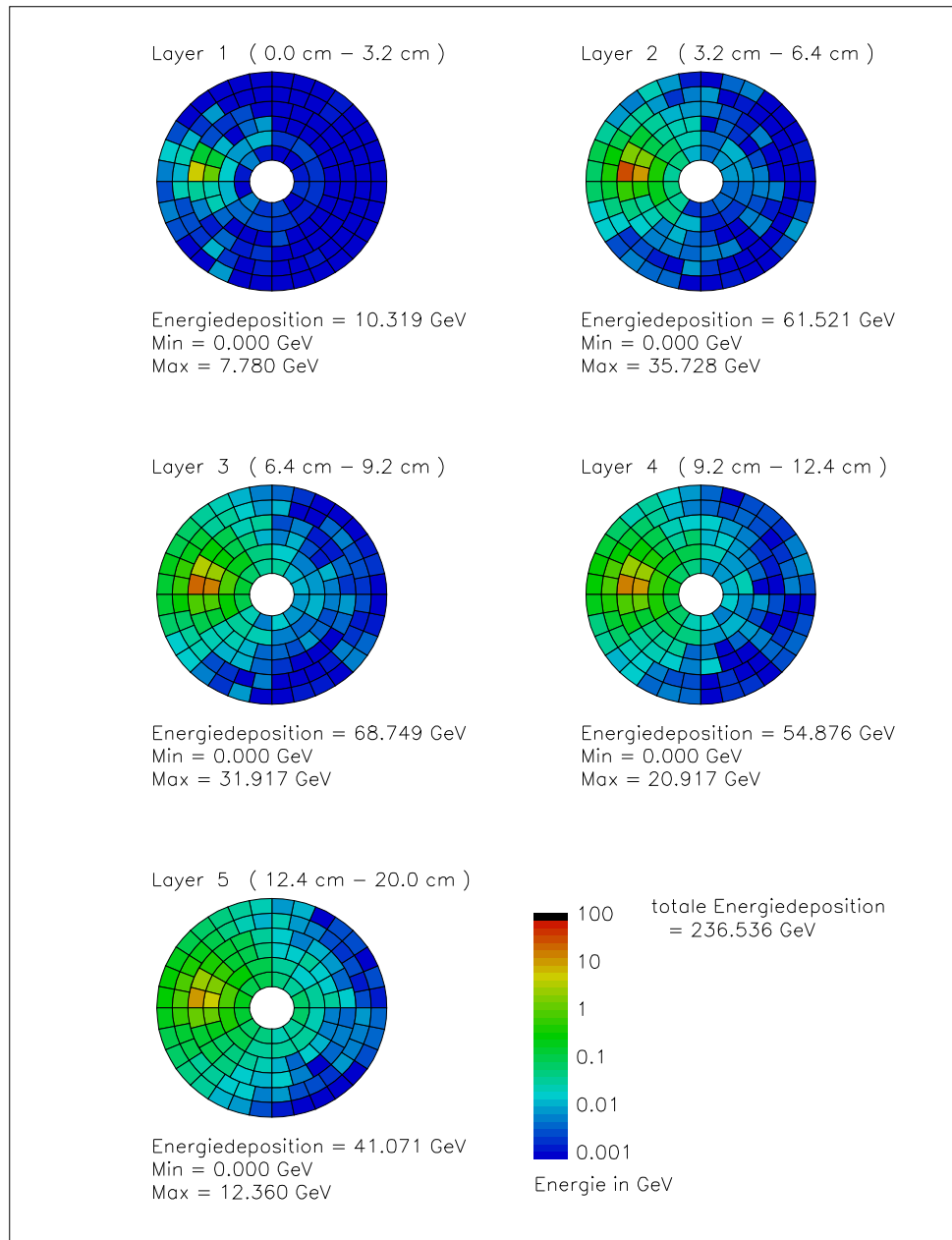


Figure 28: The energy depositions of a shower induced by a 250 GeV electron in the crystal calorimeter for several segments in depth.

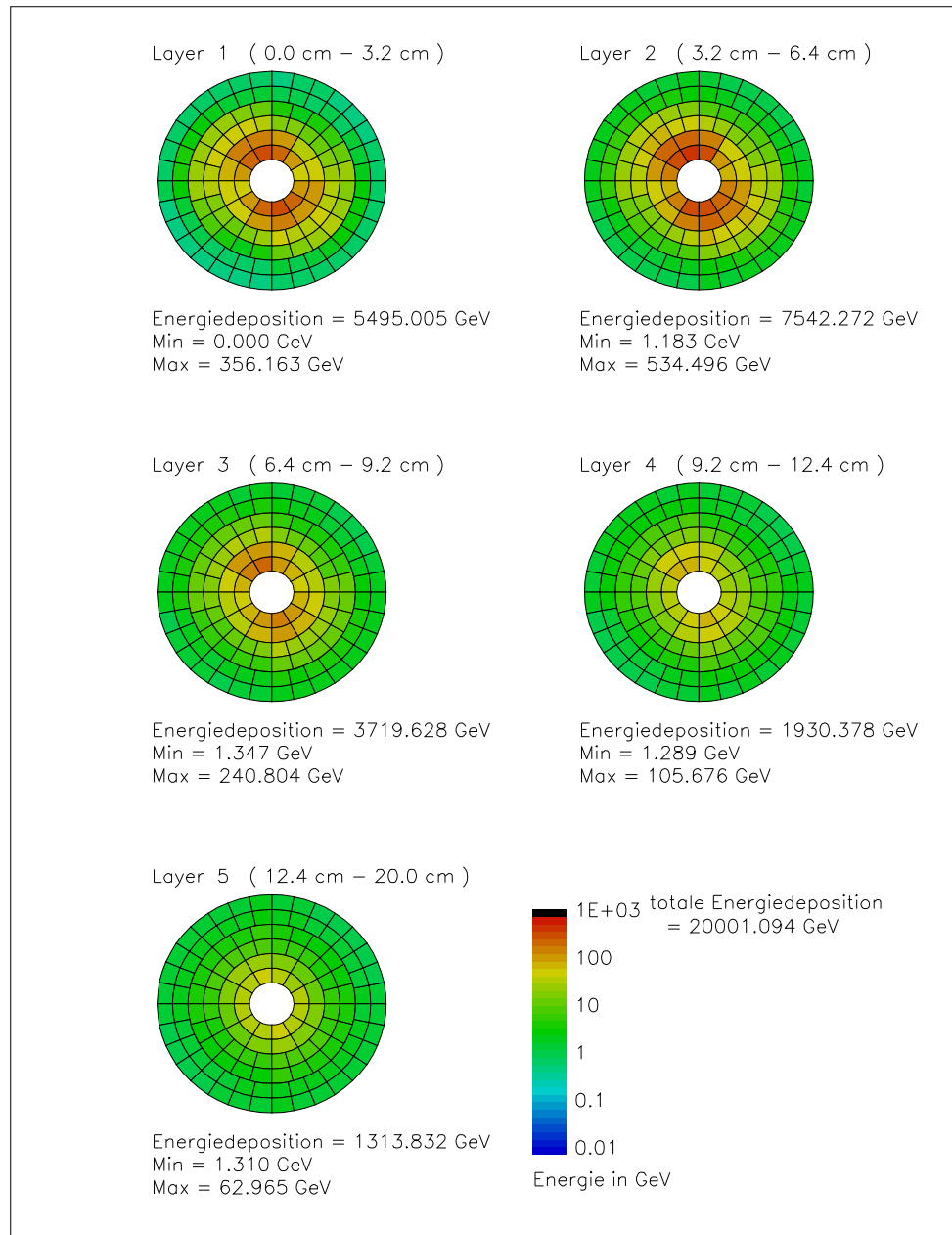


Figure 29: The energy depositions of electrons from beamstrahlung (background) in the crystal calorimeter for several segments in depth.

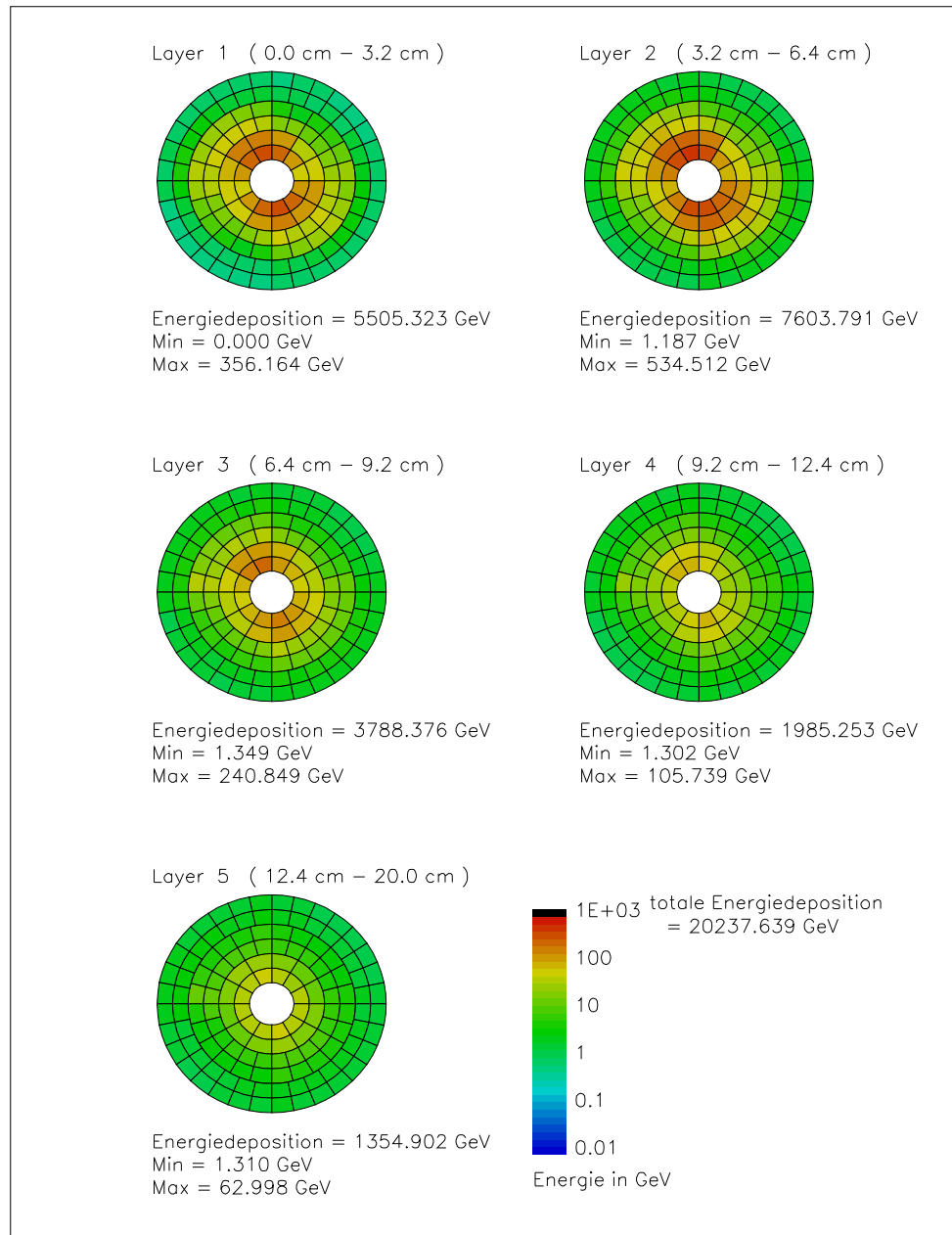


Figure 30: The superposition of the shower of an electron of 250 GeV and the electrons from beamstrahlung in the crystal calorimeter for several segments in depth.

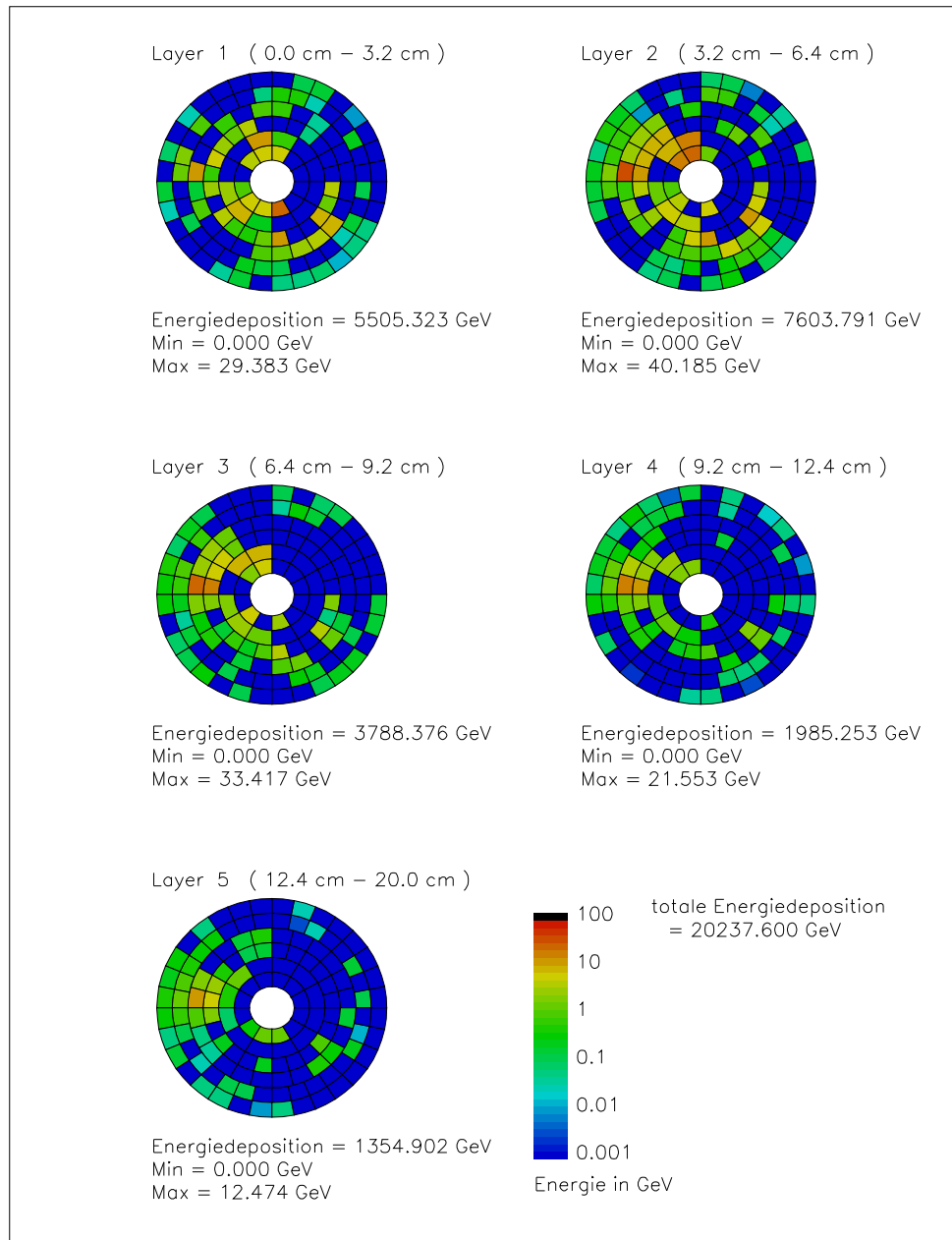


Figure 31: The difference between the depositions from an electron of 250 GeV superimposed on the background and the background obtained from the calorimeter on the opposite side.